The role of melanin pathways in extremotolerance and virulence of *Fonsecaea* revealed by *de novo* assembly transcriptomics using illumina paired-end sequencing

X.Q. Li[1], B.L. Guo[1], W.Y. Cai[1], J.M. Zhang[1], H.Q. Huang[2], P. Zhan[3,4,5], L.Y. Xi[1], V.A. Vicente[6], B. Stielow[4], J.F. Sun[7*], and G.S. de Hoog[4,5,6,8,9]

[1]*Department of Dermatology, Sun Yat-sen Memorial Hospital, Sun Yat-sen University, Guangzhou, China;* [2]*Department of Dermatology, The Third Affiliated Hospital, Sun Yat-sen University, Guangzhou, China;* [3]*Dermatology Hospital of Jiangxi Province, Nanchang, China;* [4]*CBS-KNAW Fungal Biodiversity Centre, Utrecht, The Netherlands;* [5]*Institute of Biodiversity and Ecosystem Dynamics, University of Amsterdam, Amsterdam, The Netherlands;* [6]*Basic Pathology Department, Federal University of Paraná State, Curitiba, Paraná, Brazil;* [7]*Guangdong Provincial Institute of Public Health, Guangdong Provincial Center for Disease Control and Prevention, Guangzhou, Guangdong, China;* [8]*Biological Sciences Department, Faculty of Science, King Abdulaziz University, Jeddah, Saudi Arabia;* [9]*Department of Dermatology, First Hospital of Peking University, Beijing, China*

**Correspondence*: J.F. Sun, sunjiuf@163.com

Abstract: Melanisation has been considered to be an important virulence factor of *Fonsecaea monophora*. However, the biosynthetic mechanisms of melanisation remain unknown. We therefore used next generation sequencing technology to investigate the transcriptome and digital gene expression data, which are valuable resources to better understand the molecular and biological mechanisms regulating melanisation in *F. monophora*. We performed *de novo* transcriptome assembly and digital gene expression (DGE) profiling analyses of parent (CBS 122845) and albino (CBS 125194) strains using the Illumina RNA-seq system. A total of 17 352 annotated unigenes were found by BLAST search of NR, Swiss-Prot, Gene Ontology, Clusters of Orthologous Groups and Kyoto Encyclopedia of Genes and Genomes (KEGG) (*E*-value <1e–5). A total of 2 283 unigenes were judged to be the differentially expressed between the two genotypes. We identified most of the genes coding for key enzymes involved in melanin biosynthesis pathways, including polyketide synthase (*pks*), multicopper oxidase (*mco*), laccase, tyrosinase and homogentisate 1,2-dioxygenase (*hmgA*). DEG analysis showed extensive down-regulation of key genes in the DHN pathway, while up-regulation was noted in the DOPA pathway of the albino mutant. The transcript levels of partial genes were confirmed by real time RT-PCR, while the crucial role of key enzymes was confirmed by either inhibitor or substrate tests *in vitro*. Meanwhile, numbers of genes involved in light sensing, cell wall synthesis, morphology and environmental stress were identified in the transcriptome of *F. monophora*. In addition, 3 353 SSRs (Simple Sequence Repeats) markers were identified from 21 600 consensus sequences. Blocking of the DNH pathway is the most likely reason of melanin deficiency in the albino strain, while the production of pheomelanin and pyomelanin were probably regulated by unknown transcription factors on upstream of both pathways. Most of genes involved in environmental tolerance to oxidants, irradiation and extreme temperatures were also assembled and annotated in transcriptomes of *F. monophora*. In addition, thousands of identified cSSR (combined SSR) markers will favour further genetic linkage studies. In conclusion, these data will contribute to understanding the regulation of melanin biosynthesis and help to improve the studies of pathogenicity of *F. monophora*.

Key words: Chromoblastomycosis, *Fonseca monophora*, Melanin, Paired-end sequencing, Transcriptome.

Available online 28 February 2016; http://dx.doi.org/10.1016/j.simyco.2016.02.001. Hard copy: xxx.

INTRODUCTION

The genus *Fonsecaea* comprises etiologic agents of human chromoblastomycosis, a chronic (sub)cutaneous infection eventually leading to cauliflower-like eruptions on the skin (Kombila *et al.* 1995, Esterre *et al.* 1996, Attapattu 1997, Silva *et al.* 1998, Queiroz-Telles *et al.* 2009, Xi *et al.* 2009a,b). The disease has mostly been reported in tropical and subtropical climate zones, and has a high incidence in endemic areas (Najafzadeh *et al.* 2011, Sun *et al.* 2012), but autochthonous infections have also been reported from temperate Europe (Pindycka-Piaszczynska *et al.* 2014). One of the consistent features of etiologic agents of chromoblastomycosis is their consistent melanisation, all species having an olivaceous black thallus. Upon entering human tissue, a shift is observed from hyphal to meristematic growth, leading to formation of the isodiametrically enlarging tissue phase, the muriform cell.

Published reports on melanisation of *Fonsecaea* showed that the pathogens are able to produce secreted as well as cell-wall-associated melanin-like components (Cunha *et al.* 2005, Franzen *et al.* 2006, Santos *et al.* 2007). These melanins are either immunological activators or involved in interaction with host immune cells (Farbiarz *et al.* 1992, Nosanchuk *et al.* 1998), while effects on susceptibility to antifungal agents are not congruent (Polak & Dixon 1989, van de Sande *et al.* 2007, Sun *et al.* 2011).

Fonsecaea monophora, one out of four pathogenic species of *Fonsecaea*, is able to cause subcutaneous as well as brain infections (de Hoog *et al.* 2004, Surash *et al.* 2005). In our previous study, a morphological mutant of *F. monophora* showing meristematic growth *in vivo* and *in vitro* was isolated from a case of chromoblastomycosis in China (Xi *et al.* 2009a,b). After two years of subculturing (transferred every three months) an albino mutant was obtained (Sun *et al.* 2011). The parent strain showed slow-growing, black, heaped colonies, and produced cell-wall-associated secreted melanin, while the albino mutant was melanin-deficient and was sensitive to environmental stress factors of temperature, pH, UV irradiation and oxidative stress (Sun *et al.* 2011). Moreover, melanisation of the parent strain inhibited production of nitric oxide and Th1 cytokines of murine

Peer review under responsibility of CBS-KNAW Fungal Biodiversity Centre.

Please cite this article in press as: Li XQ, et al., The role of melanin pathways in extremotolerance and virulence of *Fonsecaea* revealed by *de novo* assembly transcriptomics using illumina paired-end sequencing, Studies in Mycology (2016), http://dx.doi.org/10.1016/j.simyco.2016.02.001

macrophages, which probably enhanced persistence of the fungus in tissue (Zhang *et al.* 2013). The loss of melanin production ability in albino strain perhaps was due to the mutations of key enzymes in melanin biosynthetic pathway. Differ from those resulting from random mutagenesis or recoverable mutations generated by UV light (Romero-Martinez *et al.* 2000, Ruiz-Diez & Martinez-Suarez 2003), these mutations of key enzymes are fixed after generated from parent strain, result in permanent loss of melanin production in albino strain. Therefore, clarification of the melanin biosynthesis pathway in the albino mutant is essential to elucidate the physiological processes involved in melanisation and will help to understand the pathogenesis of *Fonsecaea*. However, large-scale identification of melanin biosynthetic pathway genes at genome or transcriptome levels is still not available in *F. monophora*.

RNA deep sequencing technologies such as Solexa/Illumina RNA-seq and Digital Gene Expression (DGE) have changed approaches in functional gene identification dramatically. These technologies greatly facilitate investigation of functional complexity of transcriptomes (Anisimov 2008, Wang *et al.* 2009). RNA-seq refers to transcriptome shotgun sequencing wherein mRNA or cDNA is mechanically fragmented, resulting in overlapping short fragments that cover the entire transcriptome. DGE is a tag-based transcriptome sequencing approach where short raw tags are generated by endonucleases. The expression level of virtually all genes in the sample is measured by counting the number of individual mRNA molecules produced from each gene. Compared with DGE analysis, RNA-seq is a powerful approach to unravel transcriptome complexity, and to identify genes, transcript structure, alternative splicing, non-coding RNAs, and new transcription units. In contrast, the DGE protocol is more suitable and affordable for comparative gene expression studies because it enables direct transcript profiling without compromise and potential bias, thus allowing sensitive and accurate profiling of the transcriptome that reflects the biology of the cell more closely (Morozova & Marra 2008, Mortazavi *et al.* 2008, Nagalakshmi *et al.* 2008, Sultan *et al.* 2008). These two technologies have increasingly been used in transcriptome profiling studies of divergent organisms (Xiang *et al.* 2010, Wei *et al.* 2011, Liu *et al.* 2012, Liang *et al.* 2013).

The present study conducts a transcriptome profiling analysis of *F. monophora* using RNA-seq and DGE to gain deep insight into melanin biosynthetic pathways, as well as in cell wall biosynthesis genes and tolerance genes responding to environmental stress (oxidants, irradiation and extreme temperatures).

MATERIAL AND METHODS

Strains and RNA extraction

CBS 122845 was isolated from lesion of an 81-year-old male patient (Xi *et al.* 2009a,b). The isolate was confirmed to be a meristematic mutant of *F. monophora* by morphology and multilocus molecular data including ITS, *ACT*, *BT2* and *CDC42* genes (Sun *et al.* 2011). Its albino mutant CBS 125194 (the mutant was initially assigned as CBS 125149, while the accession number was changed to be CBS 125194) was generated by subculture *in vitro* (once per three months) (Sun *et al.* 2011). For the transcriptome sequencing, both strains were cultured at 25 °C for 14 days on potato dextrose agar (PDA) medium. Cells were scraped from the colony surface, immediately frozen in liquid nitrogen and transferred to the sequencing company with dry ice.

Total RNA of each sample was isolated using a hexadecyltrimethylammonium bromide (CTAB) based protocol and further purified with the RNeasy Plus Universal Kits (Qiagen, Valencia, USA). RNA quality was verified using a 2100 Bioanalyzer RNA Nanochip (Agilent, Santa Clara, USA), and both samples had RNA Integrity Number (RIN) value more than 9.0. Then RNA was quantified using NanoDrop ND-1000 Spectrophotometer (NanoDrop, Wilmington, USA). A total of each 20 µg of RNA was used for cDNA library preparation.

cDNA library construction and sequencing

Illumina sequencing using the HiSeq™ 2000 platform was performed at the Beijing Genomics Institute (BGI), Shenzhen, China (www.genomics.cn/index.php) according to the manufacturer's instructions (Illumina, San Diego, USA). Briefly, poly (A) RNA was isolated from total RNA using Sera-mag Magnetic Oligo (dT) Beads (Illumina). To avoid priming bias when synthesising cDNA, purified mRNA was first fragmented into small pieces (100~400 bp) using divalent cations at 94 °C for exactly 5 min. Then the double-stranded cDNA was synthesised using the SuperScript Double-Stranded cDNA Synthesis kit (Invitrogen, Camarillo, USA) with random hexamer (N6) primers (Illumina). The synthesised cDNA was subjected to end-repair and phosphorylation using T4 DNA polymerase, Klenow DNA polymerase and T4 PNK. These repaired cDNA fragments were 3′-adenylated using Klenow Fragment (3′–5′ exo-, Illumina). Illumina paired-end adapters were ligated to the ends of these 3′-adenylated cDNA fragments. To select a size range of templates for downstream enrichment, products of the ligation reaction were purified on a 2 % TAE-agarose gel (Certified Low-Range Ultra Agarose, Biorad, USA). A range of cDNA fragments (200 ± 25 bp) was excised from the gel. Fifteen rounds of PCR amplification were performed to enrich the purified cDNA template using PCR Primers PE 1.0 and PE 2.0 (Illumina) with Phusion DNA Polymerase. The cDNA library was constructed with a fragment length range of 200~400 bp. Finally, after validating on an Agilent Technologies 2100 Bioanalyzer using the Agilent DNA 1000 chip kit (Agilent, Santa Clara, USA), the cDNA library was sequenced on a PE flow cell using Illumina HiSeq™ 2000 platform, clean sequencing reads with Q20 > 97 % were used for further analysis.

Data filtering and *de novo* assembly

Quality requirements for *de novo* transcriptome sequencing are significantly higher than that for re-sequencing, because sequencing errors can create difficulties for the short-read assembly algorithm. We therefore carried out a stringent filtering process. Firstly, we removed reads that did not pass the built-in Illumina's software Failed-Chastity filter according to the relation "failed-chastity $\leq$ 1", using a chastity threshold of 0.6, on the first 25 cycles. Secondly, we discarded all reads with adaptor contamination. Thirdly, we ruled out low-quality reads with ambiguous sequences "N". Finally, the reads with more than 10 % Q < 20 bases were also removed.

De novo assembly was carried out with the Trinity short reads assembling program (http://trinityrnaseq.sourceforge.net/)

Please cite this article in press as: Li XQ, et al., The role of melanin pathways in extremotolerance and virulence of *Fonsecaea* revealed by *de novo* assembly transcriptomics using illumina paired-end sequencing, Studies in Mycology (2016), http://dx.doi.org/10.1016/j.simyco.2016.02.001

(Release-20130225). This program combines three independent software modules: INCHWORM, CHRYSALIS, and BUTTERFLY, applied sequentially to process large volumes of RNA-seq reads. Trinity partitions the sequence data into many individual de Bruijn graphs (de Bruijn 1946), each representing the transcriptional complexity at a given gene or locus, and then processes each graph independently to extract full-length splicing isoforms and to tease apart transcripts derived from paralogous genes. Assembled RNA-seq data were generated as unique sequences of transcripts using Inchworm, often yielding full-length transcripts for a dominant isoform, but then just the unique portions of alternatively spliced transcripts were reported. Secondly, Inchworm arranges the contigs into clusters and constructs complete de Bruijn graphs for each cluster using Chrysalis. Each cluster represents the full transcriptional complexity for a given gene. Chrysalis then partitions the full read set among these disjoint graphs. Thirdly, the individual graphs were processed in parallel, tracing the path that reads and pairs of reads take within the graph using BUTTERFLY, ultimately reporting full-length transcripts for alternatively spliced isoforms, and separating transcripts that correspond to paralogous genes (Grabherr *et al.* 2011).

The sequences resulting from Trinity are called unigenes, further processing the assembly of each sample with a further process of sequence splicing and redundancy removing, using clustering software to acquire non-redundant unigenes as long as possible. Subsequently gene family clustering is done, dividing the unigenes in two classes. One consists of clusters (with prefix CL), showing the cluster ID behind. A single cluster comprises several unigenes with similarities >70 %. The other consists of singletons, having the prefix unigene. In a final step, blastx alignment was performed. For identifying potential protein products encoded by nucleotide query, the unigenes were firstly translated to six potential amino acid sequences, and then aligned with known protein data (v2.2.26+x64-linux) (*E*-value < 0.00001) between unigenes and protein databases NR, Swiss-Prot, KEGG, and COG, and the best alignments were used to determine sequence direction of unigenes. If results of databases were in conflict, a priority order of NR, Swiss-Prot, KEGG and COG was followed. When unigenes were unalignable with any of the databases, software package ESTScan (v3.0.2) (Iseli *et al.* 1999) was introduced to decide on sequence direction. Unigenes with directions are provided as 5′–3′-ends, whereas for those without direction, sequences were taken out from assembly software.

Unigene function annotation, GO classification, pathway analysis

For validation and annotation of assembled unigenes, sequence similarity search was conducted against NR, the Swiss-Prot protein, KEGG, COG and two closely species (*F. pedrosoi*, *F. multimorphosa*) genome data on Broad institute using blastx alignment with an *E*-value threshold of 10^{-5}. The KEGG database contains a systematic analysis of intracellular metabolic pathways and functions and enhances pathway annotation of unigenes (Path-finder; http://www.genome.jp/) (Kanehisa *et al.* 2008). COG is a database where orthologous genes are classified, assuming that every protein has evolved from an ancestor protein. NT is the non-redundant NCBI nucleotide database, with entries from all traditional divisions of GenBank, EMBL, and DDBJ excluding bulk divisions.

Gene Ontology (GO) functional annotation has three ontologies: molecular function, cellular component and biological process. With NR annotation, we used the program Blast2GO (v2.5.0) to get GO annotation of unigenes (Conesa *et al.* 2005). After obtaining GO annotation for every unigene, we used WEGO software (www.wego.genomics.org.cn) to perform GO functional classification for all unigenes and to understand the distribution of gene functions of the species from the macro level (Ye *et al.* 2006).

Unigene expression difference analysis

This analysis aims to predict genes with different expression levels, subsequently carrying out GO functional analysis and KEGG pathway analysis. Unigene expression calculations were aided by FPKM (Fragments Per kb per Million reads) (Audic & Claverie 1997) which were used to eliminate the influence of differences in gene lengths and sequencing level. Accordingly, verified gene expressions could be used directly for comparison of differences in gene expression between samples. The formulae of FPKM and RPKM are identical (Fig. 1A), If both pairs of reads were aligned to a gene, we treated them as a single fragment with FPKM; otherwise they were treated as two reads with RPKM.

We developed a rigorous algorithm to identify differentially expressed genes between two samples (Fig. 1B). The null hypothesis and alternative hypothesis to identify expressed genes between two samples are defined as follows: H_0 = a gene with the same expression level in two samples; H_1 = a gene with different expression levels in two samples. The probability of gene A expressed equally between two samples can then be calculated with the following formula (Fig. 1C).

With thousands of hypotheses tested, the suitable *p*-value for an individual test is insufficient to guarantee a low rate of false discovery. There we had to do multiple testing corrections for each individual hypothesis to guarantee a low false discovery rate in the entire dataset. FDR (False Discovery Rate) control is a statistical method used in multiple hypotheses testing to correct for *p*-value. In practical terms, the FDR is the expected false discovery rate

A

$$FPKM = \frac{10^6 C}{NL/10^3}$$

B

$$p(x) = \frac{e^{-\lambda}\lambda^x}{x!}$$

C

$$p(i \mid x) = \left(\frac{N_2}{N_1}\right)^i \frac{(x+i)!}{x!i!\left(1+\frac{N_2}{N_1}\right)^{(x+i+1)}}$$

D

$$P = 1 - \sum_{i=0}^{m-1} \frac{\binom{M}{i}\binom{N-M}{n-i}}{\binom{N}{n}}$$

Fig. 1. The formulae involved in this study. The formulae used for unigene expression level calculation (A), *N*: the total number of fragments that uniquely aligned to all unigenes, *C*: the number of fragments that uniquely aligned to particular unigenes, *L*: nucleotides numbers. The formulae used for differentially expressed genes identification (B), *x* as the number of fragments that can uniquely map to target gene, λ is the transcript of particular gene. The formulae used for probability of particular gene between two samples calculation. N_1: the total number of fragments in sample 1, N_2: the total number of fragments in sample 2, *x*: particular gene holds fragments in sample 1, *i*: particular gene holds fragments in sample 2. The hyper-geometric tests used for significantly enriched GO terms in DEGs comparing to the genome background (D), *N* is the number of all genes with GO annotation, *n* is the number of DEGs in *N*, *M* is the number of all genes that are annotated to the certain GO terms, and *m* is the number of DEGs in *M*.

Please cite this article in press as: Li XQ, et al., The role of melanin pathways in extremotolerance and virulence of *Fonsecaea* revealed by *de novo* assembly transcriptomics using illumina paired-end sequencing, Studies in Mycology (2016), http://dx.doi.org/10.1016/j.simyco.2016.02.001

(Benjamini *et al.* 2001). In our analysis, we choose those with FDR $\leq$0.001 and logarithmic ratio (FPKM) larger than 1.

GO classification of differentially expressed unigenes and pathway analysis

GO functional analyses provide functional classification annotation and enrichment analysis for DEGs (Differentially Expressed Genes). First, mapping was done of all differentially expressed genes to each term of the Gene Ontology database (www.geneontology.org/) and calculating the gene numbers of each GO term. Subsequently, hyper-geometric tests were used to find significantly enriched GO terms in DEGs comparing to the genome background. The formula calculating a *p*-value in this hypothesis test is as in Fig. 1D. The calculated *p*-value goes through Bonferroni Correction, assuming a corrected *p*-value $\leq$0.05 as a threshold. GO terms fulfilling this condition were defined as significantly enriched GO terms in DEGs. This analysis was able to recognise the main biological functions that DEGs exercise. Our GO functional enrichment analysis also integrated clustering analysis of expression patterns. Thus, expression patterns of DEGs annotated to a given GO-term were obtained relatively easily.

Pathway enrichment analysis identifies significantly enriched metabolic pathways or signal transduction pathways in DEGs comparing the entire genome background. The calculating formula of *p*-value is the same as in GO analysis (Fig. 1D). Here *N* is the number of all genes with KEGG annotation, *n* is the number of DEGs in *N*, *M* is the number of all genes annotated to specific pathways, and m is number of DEGs in M. After multiple testing corrections, we observed pathways with *Q*-values $\leq$0.05 being significantly enriched in DEGs.

Development of cDNA-derived SSR markers

A Perl script known as MIcroSAtellite (www.pgrc.ipk-gatersleben.de/misa/) was used to identify microsatellites in the unigenes. In this study, cDNA-based SSRs (Simple Sequence Repeats) were considered to contain motifs with two to six nucleotides in size and a minimum of 4 contiguous repeat units. Frequency of cSSR refers to kilobase pairs of cDNA sequences containing one SSR.

Confirmation of genes transcript using Real time RT-PCR

Thirty-six assembled genes distributed in melanin synthesis, light sensing, cell wall synthesis, morphology regulation and environmental resistant pathways (UV, temperature, oxidative stress) were selected for DEG data confirmation. The primers were designed using Primer Premier 5.0 software (Premier Biosoft International, Palo Alto, USA), and all the primers were synthesised in Life Technology Company (Life Technology, Shanghai, China) (Table S1). Total RNA of both strains was extracted as our previous described (Liu *et al.* 2007, Sun *et al.* 2014). 500 ng precipitated RNA was used for cDNA synthesis using PrimeScript™ RT reagent Kit (TaKaRa, Dalian, China). Real-time PCR reactions were performed using SYBR ExScript™ RT-PCR Kit (TakaRa). The cycling conditions were 95 °C for 30 s, followed by 45 repetitive cycles at 95 °C for 5 s, 60 °C for 10 s. A melting curve analysis was performed from 65 °C to 95 °C. *ACT* (unigene7394) was used as the internal normalise gene. The specific amplification of each gene was confirmed by melting curve analysis. Results analyses were same as our described before (Liu *et al.* 2007, Sun *et al.* 2014).

DHN inhibitor test, laccase, tyrosinase activity assays and light-sensor test

Tricyclazole was used as inhibitor of pentaketide melanin biosynthesis to evaluate the pathway of DHN melanin synthesis (Franzen *et al.* 2006). All strains were cultured PDA medium with 50 mg/L tricyclazole at 25 °C for 7 days.

Laccase and tyrosinase enzymes activities were tested according to Laufer *et al.* (2006). Both strains were cultured on PDA medium at 25 °C for 7 days. Total protein extraction and purification were carried out as described previously. 2,2-azino-bis-(3-ethylbenzthiazolinsulfonate) (ABTS) (Sigma) and syringaldazine (Sigma) were used as substrate of laccase activity test, while DOPA (Sigma) and tyrosine (Sigma) were used as substrate of tyrosinase as described by Laufer *et al.* (2006).

For the light effects experiment, both strains were grown on PDA medium (Chen *et al.* 2014). Cultures were exposure to a light and incubated at 25 °C for 7 days.

RESULTS AND DISCUSSION

Sequencing and transcriptome assembly

To obtain a global overview of the transcriptome and gene activity at nucleotide resolution of parent (CBS 122845) and albino mutant strain (CBS 125194), each three independent cDNA libraries were constructed and sequenced separately using an Illumina HiSeq2000 genome analyzer. After stringent quality check and data cleaning, more than 143 million clean reads were obtained from each sample (Q20 bases >97 %, G+C about 53 %) (Table 1). The total length in nucleotides was

Table 1. Summary of reads in melanised strain and albino strain of *F. monophor*a, and statistics of assembly quality.

	CBS 122845	CBS 125194
Total reads	15 36 78 424	14 35 01 576
Total clean reads	15 05 29 368	14 04 47 326
Total clean nucleotides (nt)	15 05 29 36 800	14 04 47 32 600
Q20	97.42 %	97.31 %
N	0.00 %	0.00 %
GC	53.60 %	53.36 %
Contig total number	26 939	27 267
Contig total length (nt)	2 54 82 551	2 60 50 225
Contig mean length (nt)	945	955
N50	2 273	2 370

Total reads and total nucleotides are clean reads and clean nucleotides.
Total nucleotides should be more than contract provision.
Q20 percentage is proportion of nucleotides with quality value larger than 20.
N percentage is proportion of unknown nucleotides in clean reads.
GC percentage is proportion of guanidine and cytosine nucleotides among total nucleotides.
Total clean nucleotides = total clean reads1 x read1 size + total clean reads2 × read2 size.

Please cite this article in press as: Li XQ, et al., The role of melanin pathways in extremotolerance and virulence of *Fonsecaea* revealed by *de novo* assembly transcriptomics using illumina paired-end sequencing, Studies in Mycology (2016), http://dx.doi.org/10.1016/j.simyco.2016.02.001

29 097 669 400 nt. After assembly with Trinity, 26 939 contigs for CBS 122S845, and 27 267 contigs for CBS 125194 were obtained with an average lengths of ~950 bp and N50 of ~2 300 bp, respectively. The lengths of contigs ranging between 200 and 3 000 bp accounted for 97 % of all contigs, and the remainder reached more than 3 000 bp (~3 %). In total, 21 600 consensus unigenes were generated with mean lengths of 2 305 bp and N50 of 3 385 bp (Table 2). The divergence of three biological replicates for each strain and between two strains was evaluated using scatter plot of gene expression (Fig. S1), the results indicated that consistency of within three replicates is significantly higher than between two strains, thus, these data indicated that throughput and sequencing quality was sufficient for further analysis.

Functional annotation

Functional annotation indicated that out of 21 600 unigenes, 17 352 (80.33 %) were annotated in the NR, the Swiss-Prot protein, KEGG, COG database. Among which, 17 138 (79.34 %) showed similarity to known proteins in the NR database, and 55.7 % of these hits showed similarities >60 % (Fig. 2A). The *E*-value frequency distribution of significant hits (*E*-value $\leq$ 1.0E−45) showed that 78.4 % of the sequences shared strong homologies (Fig. 2B). The blast hits were 12 516 (57.94 %), 12 360 (57.22 %), and 10 013 (46.36 %), when searching against Swiss-Prot, KEGG and COG databases, respectively. The most closely species in the NR database is *Exophiala dermatitidis* (NIH 8656) (63.7 %) (Fig. 2C). The annotation using above two *Fonsecaea* species genome data showed that 18 241 (84.44 %) unigenes were annotated, while 889 extra annotated genes in those two *Fonsecaea* species genomes compare with the NR database were hypothetical genes.

Protein coding region predictions of consensus unigene hits 17 021 CDS when they were aligned by blastx (*E*-value <10^{-5}) to protein databases in the priority order of NR, Swiss-Prot, KEGG, and COG. The remaining unigenes that had no matches in either the NR or other databases underwent gene prediction analysis using ESTScan, and 575 unigenes were identified using ORF prediction. In total, 81.46 % (17 596) of the putative protein coding unigenes were detected by homology analysis using the NR and Swiss-Prot, KEGG, COG databases or ESTScan predictions.

Table 2. Summary of assembled unigenes in this study.

	CBS 122845	CBS 125194	All
Unigenes total number	22 550	22 208	21 600
Unigenes total length (nt)	3 53 58 453	3 56 77 853	4 97 96 867
Unigenes mean length (nt)	1 568	1 606	2 305
N50	2 646	2 753	3 385
Total consensus sequences	22 550	22 208	21 600
Distinct clusters	5 783	5 636	10 541
Distinct singletons	16 767	16 571	11 059

Total consensus sequences represents the all assembled Unigenes.
Distinct clusters represents the cluster Unigenes. The same cluster contains some highly similar (more than 70 %) Unigenes, and these may come from the same or a homologous gene.
Distinct singletons represents the Unigenes come from a single gene.

We used the Blast2GO program to get GO annotation of unigenes and WEGO software to do GO functional classification for all unigenes. Based on the NR annotation, 17 138 unigenes were assigned gene ontology terms. GO-annotated unigenes belonged to the biological processes, cellular components, and molecular functions clusters were distributed in 46 categories (Fig. 3). Among the biological processes category, metabolic processes (3 475, 20.28 %) composed the most dominant group, followed by cellular processes (3 063, 17.72 %), single-organism processes (1 602, 9.35 %) and localisation (1 282, 7.48 %) (Fig. 3). Regarding molecular functions, 23.51 % (4 030) of the unigenes were assigned to catalytic activity, followed by binding (2 682, 15.65 %), transporter activity (694, 4.05 %) and structural molecule activity (99, 0.58 %) (Fig. 3). Among the cellular components category, cell (1 404, 8.19 %) and cell part (1 404, 8.19 %) were the dominant groups, followed by organelles membrane (1 376, 8.03 %) and (946, 5.52 %) (Fig. 3). In addition, all unigenes were subjected to a search against the COG database for functional prediction and classification. Similarly, all unigenes were assigned to COG classifications (Fig. 4). COG-annotated putative proteins were functionally classified into 25 molecular families such as cellular structure, biochemistry metabolism, molecular processing, and signal transduction (Fig. 4). The cluster for general function prediction represented the largest group (4 415, 25.76 %), followed by carbohydrate transport (2 303, 13.44 %), amino acid transport (2 033, 11.86 %), inorganic ion transport (1 710, 9.98 %) and secondary metabolites catabolism (1 401, 8.17 %). Only a few unigenes were assigned to nuclear structure and extracellular structure (14 and 40 unigenes, respectively) (Fig. 4).

The KEGG database was used to analyse potential involvement of the consensus sequences in cellular metabolic pathways. Among the 17 138 annotated genes, 12 360 could be grouped into according to the KEGG database. The unigenes were grouped into 108 cellular metabolic or signalling pathways including cellular growth, differentiation, apoptosis, migration, endocrine functions, and numerous biosynthesis metabolic pathways (data not shown).

Differentially expressed unigenes

Compared with the parent strain, we obtained 2 283 significantly differentially expressed genes between the two samples judged by using the threshold of false discovery rate (FDR $\leq$ 0.001) and the absolute value of log2 ratio $\geq$1, including 1 316 up-regulated and 967 down-regulated genes (Fig. 5).

GO functional analysis showed that these unigenes belonged to three functional clusters and were distributed in 41 categories based on the NR annotation (data not shown). To explore the biological function of the significantly differentially expressed genes, all 2 283 genes were mapped to the KEGG database, and then the hit genes were enriched to important pathways such as metabolism and signal transduction. There were 907 unigenes mapped to 96 pathways. Specific pathways were observed that are involved in metabolic pathways, biosynthesis of secondary metabolites, RNA transport, TCA cycle, and cell cycle. Interestingly, the majority of genes mapping to the above pathways were dramatically up-regulated in the albino strain which indicated more biological relevance to growth and reproduction. In particular, genes involved in phenylpropanoid biosynthesis pathways which related to melanin production were also

Please cite this article in press as: Li XQ, et al., The role of melanin pathways in extremotolerance and virulence of *Fonsecaea* revealed by *de novo* assembly transcriptomics using illumina paired-end sequencing, Studies in Mycology (2016), http://dx.doi.org/10.1016/j.simyco.2016.02.001

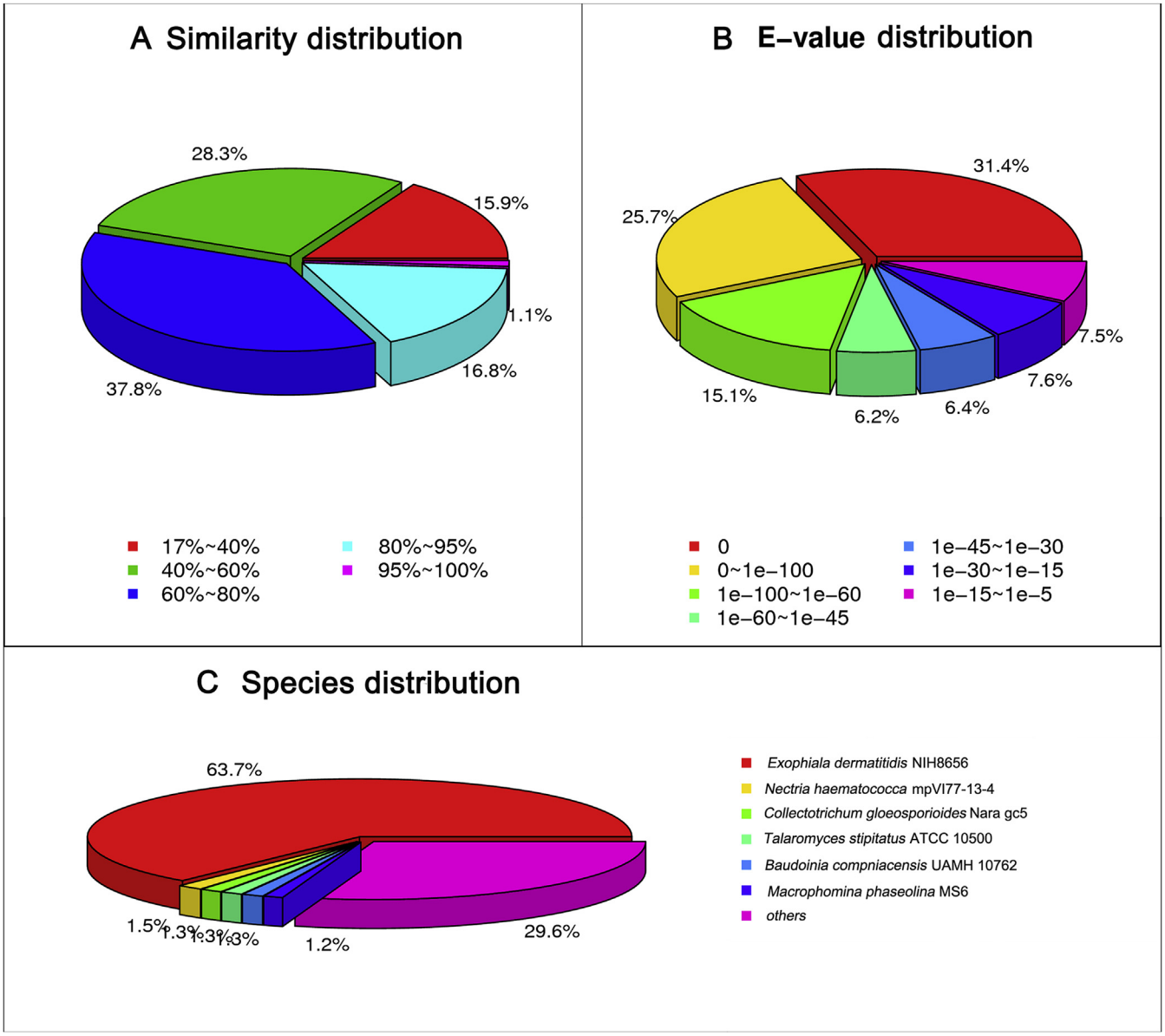

Fig. 2. *E*-value, similarity and species distribution of the top BLASTx hits against the NR database for each unigene.

substantially up-regulated. These results seem inconsistent with melanin deficiency in the albino mutant which drives us for further analysis.

Melanin biosynthesis pathway and regulation

Fungal melanins are negatively charged, hydrophobic, high molecular weight polymers which arise by oxidative polymerisation of phenolic and/or indolic precursors (Nosanchuk & Casadevall 2003). The polymers help to defend against diverse environmental stresses such as UV radiation, oxidising agents, and extreme temperatures (Jacobson 2000, Langfelder *et al.* 2003). Melanins are consistently present in the fungal agents of chromoblastomycosis (Schnitzler *et al.* 1999, Kogej *et al.* 2004, Santos *et al.* 2007, Thornton *et al.* 2015), as well as in fungi that otherwise have hyaline cell walls, e.g. *Candida albicans* (Morris-Jones *et al.* 2005), *Cryptococcus neoformans* (Chaskes *et al.* 2014), *Paracoccidioides brasiliensis* (Gomez *et al.* 2001), *Histoplasma capsulatum* (Nosanchuk *et al.* 2002), *Blastomyces dermatitidis* (Nosanchuk *et al.* 2004), and *Aspergillus fumigatus* (Tsai *et al.* 2001). Three different pathways contribute to melanin production: the DHN-melanin pathway (Fig. 6), the DOPA-melanin pathway (Fig. 7), and the L-tyrosine degradation pathway (Fig. 8) (Langfelder *et al.* 2003). The DHN-melanin biosynthetic pathway is the best characterised pathway for producing fungal eumelanin, a black pigment localised in cell walls (Wheeler *et al.* 2008). All the enzymes of the DHN-melanin pathway were found in the transcriptome of both strains (Table 3), including polyketide synthase (*pks*), α/β hydrolase (*ayg1*), scytalone dehydratase (*arp1*), 1,3,6,8-tetrahydroxynaphthalene reductase (*arp2*), multicopper oxidases (*abr1*), and ferroxidase (*abr1*) (Table 3). Polyketide synthase and the α/β hydrolase are essential for melanin production in many black fungi (Wheeler *et al.* 2008). In total, three *pks* and two *ayg1* gene homologues were found in both samples. Most of the genes in the DHN-melanin pathway were down-regulated in the albino mutant, which suggests that the DHN-melanin pathway might have been blocked, resulting in loss of melanin production (Fig. 6A). The down-regulated transcription level of partial genes was confirmed by real time RT-PCR (Fig. 6B). The inhibition test using tricyclazol showed significant decrease of DHN melanin in the parent strain, while no effects were noted in

Please cite this article in press as: Li XQ, et al., The role of melanin pathways in extremotolerance and virulence of *Fonsecaea* revealed by *de novo* assembly transcriptomics using illumina paired-end sequencing, Studies in Mycology (2016), http://dx.doi.org/10.1016/j.simyco.2016.02.001

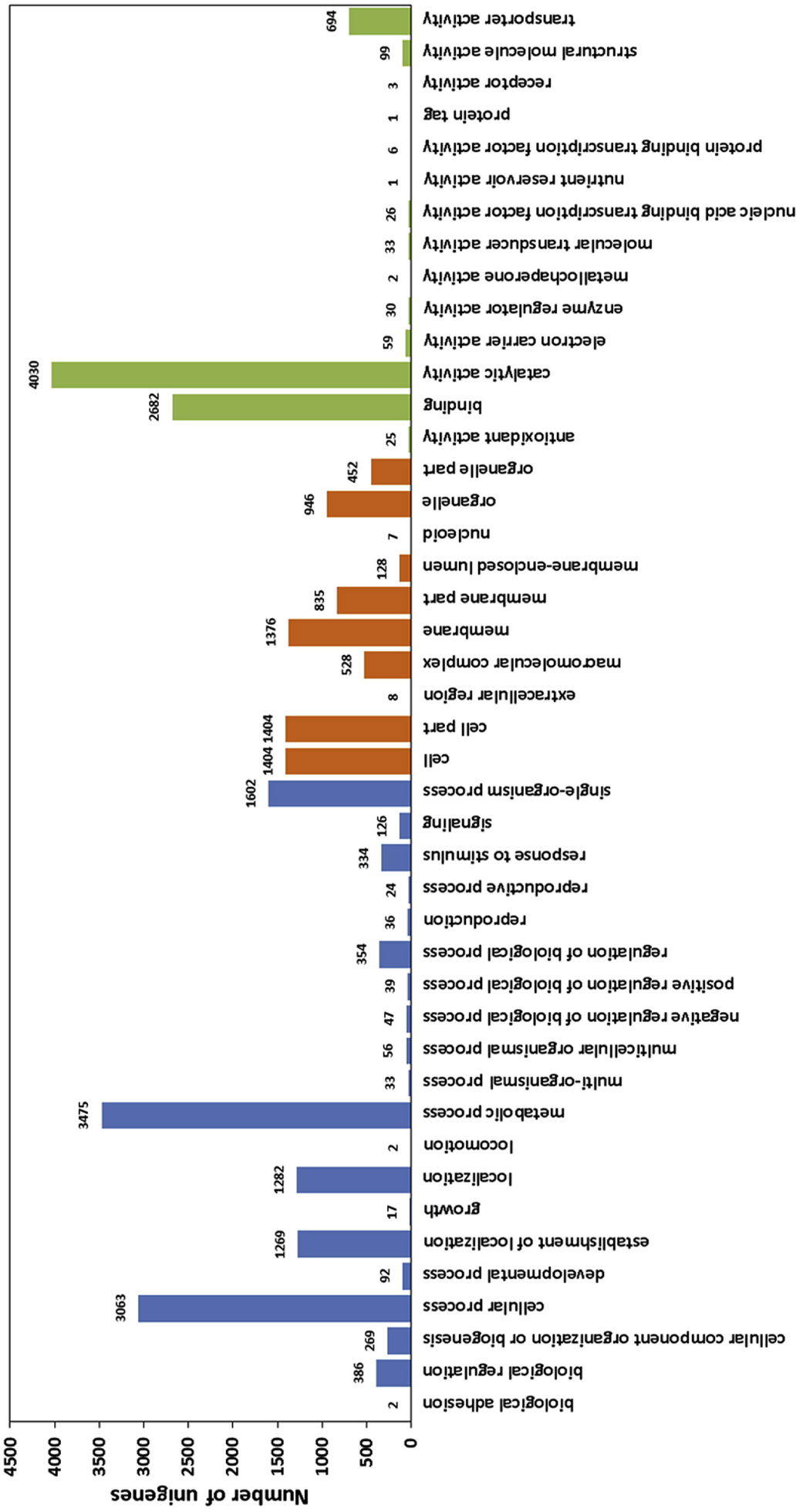

Fig. 3. GO annotations of non-redundant consensus sequences. Best hits were aligned to the GO database, and 6 876 transcripts were assigned to at least one GO term. Most consensus sequences were grouped into three major functional categories, namely biological process, cellular component, and molecular function.

Please cite this article in press as: Li XQ, et al., The role of melanin pathways in extremotolerance and virulence of *Fonsecaea* revealed by *de novo* assembly transcriptomics using illumina paired-end sequencing, Studies in Mycology (2016), http://dx.doi.org/10.1016/j.simyco.2016.02.001

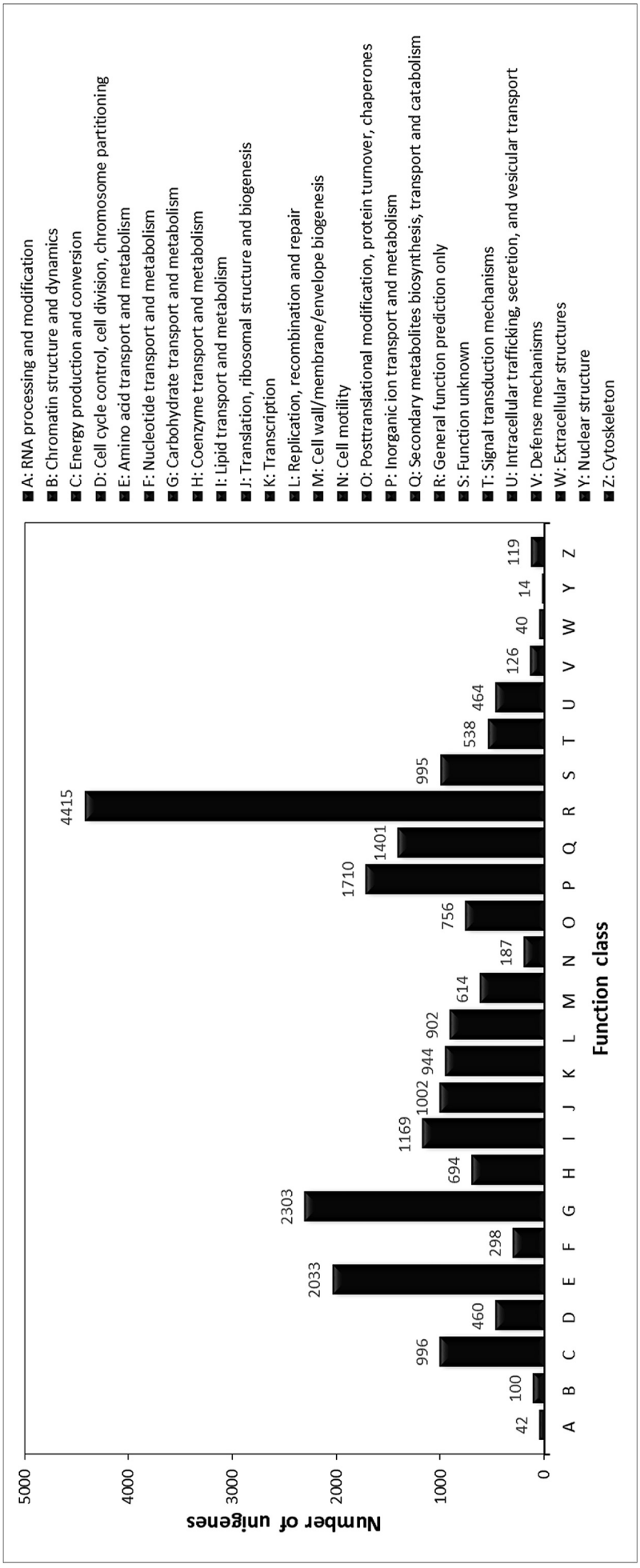

Fig. 4. Histogram presentation of clusters of orthologous groups (COG) classification. All unigenes were aligned to COG database to predict and classify possible functions.

Please cite this article in press as: Li XQ, et al., The role of melanin pathways in extremotolerance and virulence of *Fonsecaea* revealed by *de novo* assembly transcriptomics using illumina paired-end sequencing, Studies in Mycology (2016), http://dx.doi.org/10.1016/j.simyco.2016.02.001

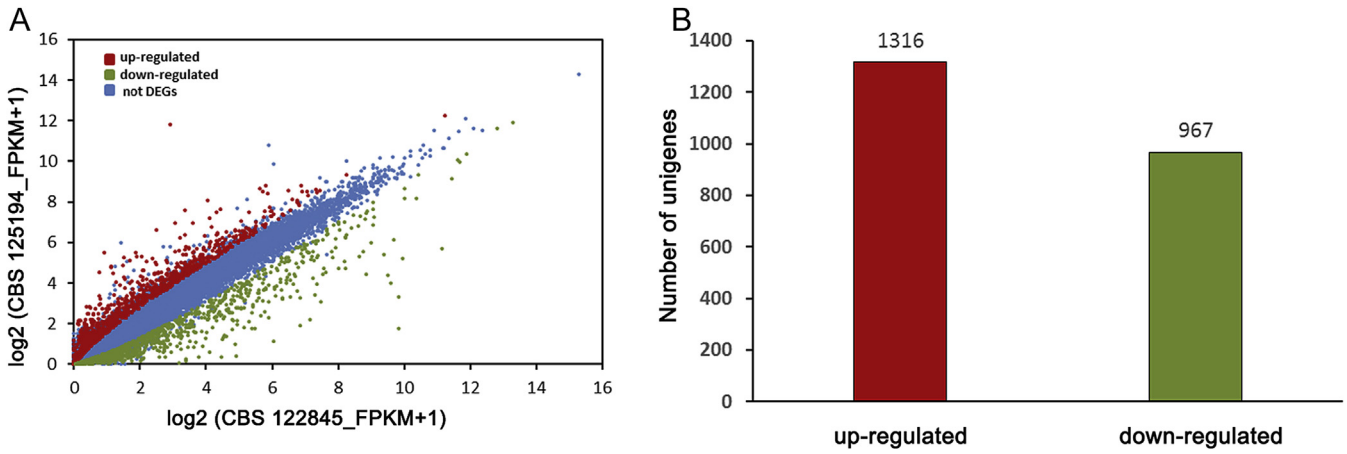

Fig. 5. Algorithm to identify differentially expressed genes between two samples (A). In the follow figure, CBS 122845 is control and CBS 125194 is treated. The genes were classified into three classes. Red genes are up-regulated that gene expression of right sample is larger than left sample. Green genes are down-regulated that gene expression of left sample is larger than right sample. Blue genes are not differentially expressed genes. The horizontal coordinate is the expression level of right and the vertical coordinate is the expression level of left sample. The distribution of Differentially Expressed Genes (DEGs) (B). The X-axis is the treat/control, and the Y-axis is the number of the DEGs. The red bar is up-regulated genes, and the green bar is down-regulated genes.

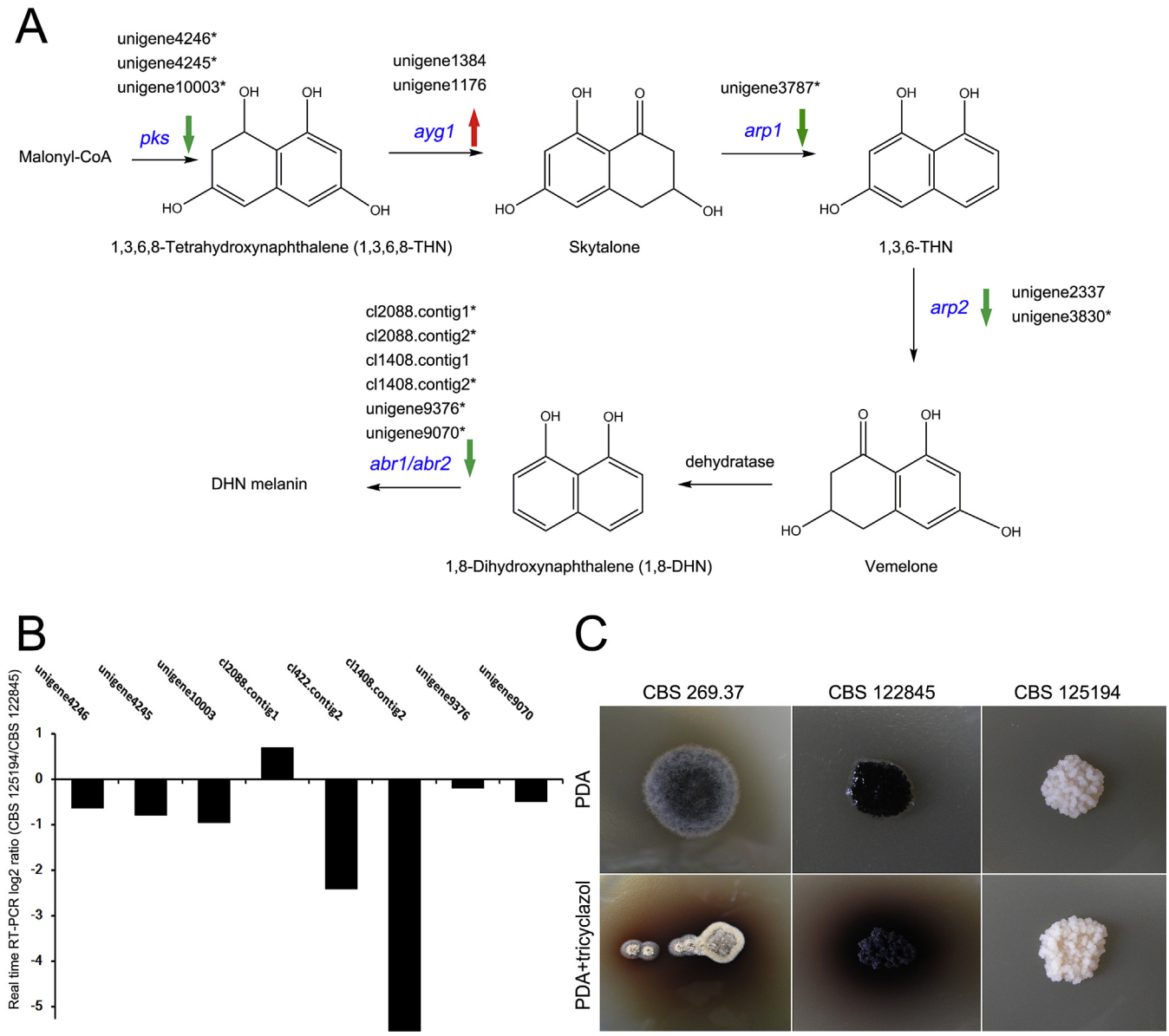

Fig. 6. The DHN-melanin pathway. The flowchart of the DHN-melanin pathway and transcription level of particular genes (blue) detected in this study (A), Red colour arrow marked up-regulated genes, while green colour arrow marked down-regulated genes. The differential expression genes supported by statistical analysis were marked as star. Transcription levels of partial genes between two strains were confirmed by Real time RT-PCR (B). The X-axis is the selected unigenes, Y-axis is the value of log2 ratio; positive value means up-regulation in albino strain compare with parent strain. DHN pathway inhibition test (C). Tricyclazole was used as inhibitors to study the pathway of melanin synthesis both strains were culture in PDA medium supplied with 50 mg/L tricyclazole. The type strain of *F. monophora* (CBS 269.37) was used as the control.

Please cite this article in press as: Li XQ, et al., The role of melanin pathways in extremotolerance and virulence of *Fonsecaea* revealed by *de novo* assembly transcriptomics using illumina paired-end sequencing, Studies in Mycology (2016), http://dx.doi.org/10.1016/j.simyco.2016.02.001

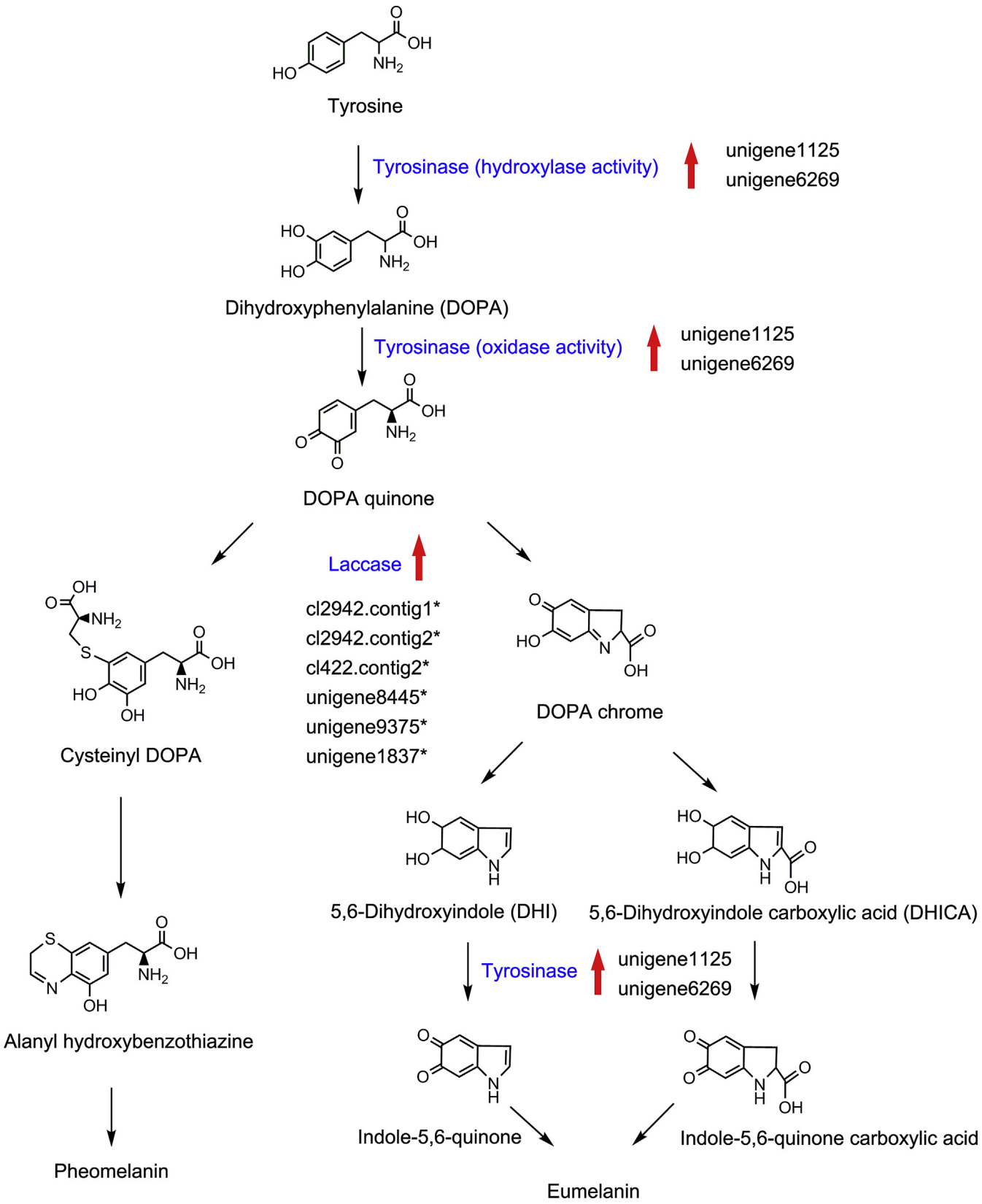

Fig. 7. The DOPA-melanin pathway. The flowchart of the DOPA-melanin pathway and transcription level of particular genes (blue) detected in this study, Red colour arrow marked up-regulated genes, while green colour arrow marked down-regulated genes. The differential expression genes supported by statistical analysis were marked as star.

the albino mutant (Fig. 6C). However, the tricyclazol could not completely inhibited the melanin production in parent strain or control strain (*F. monophora* CBS 269.37), alternatively, others melanin pathways were probably active simultaneously in parent and control strain (Fig. 6C). Both *arp1* and *arp2* are single copy in *F. monophora*. In contrast, oxidases *abr1* and *abr2* each have multiple homologous genes in the transcriptome. Multicopper oxidases (*mco*) are over-represented in *F. monophora*, including *ABR*-like pigment-related oxidases, fungal ferroxidase and laccases. A total of 14 multicopper oxidase genes were annotated in the two transcriptomes of *F. monophora* (Table 3). These *mco* genes were classified into fungal pigment multi copper oxidase

Please cite this article in press as: Li XQ, et al., The role of melanin pathways in extremotolerance and virulence of *Fonsecaea* revealed by *de novo* assembly transcriptomics using illumina paired-end sequencing, Studies in Mycology (2016), http://dx.doi.org/10.1016/j.simyco.2016.02.001

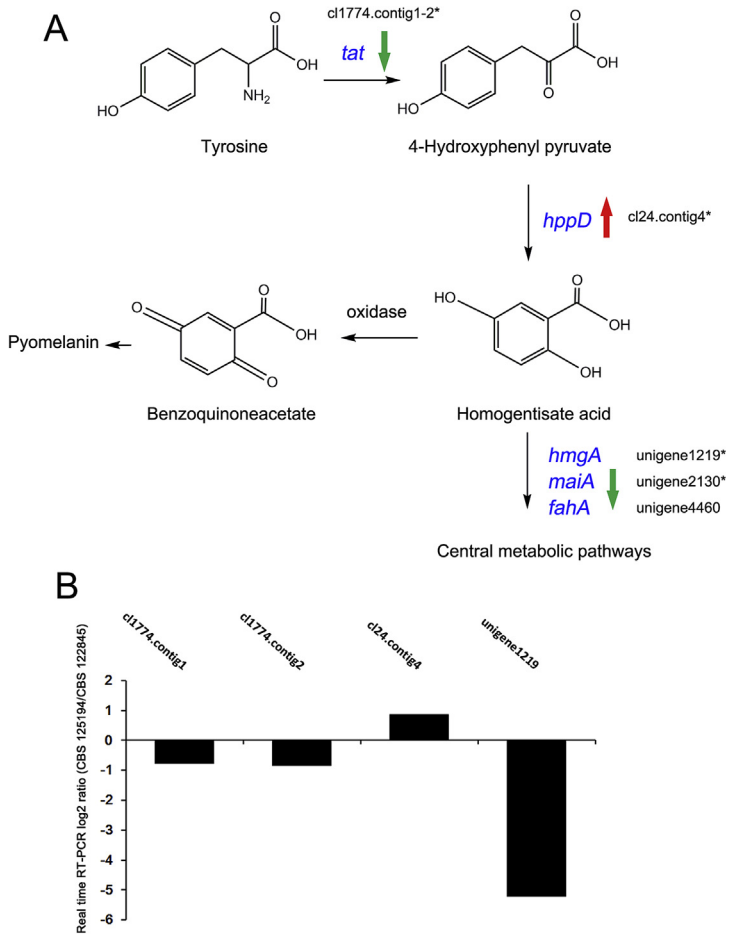

Fig. 8. The L-tyrosine degradation pathway. The flowchart of the DOPA-melanin pathway and transcription level of particular genes (blue) detected in this study (A), Red colour arrow marked up-regulated genes, while green colour arrow marked down-regulated genes. The differential expression genes supported by statistical analysis were marked as star. Transcription levels of partial genes between two strains detected by Real time RT-PCR (B). The X-axis is the selected unigenes, Y-axis is the value of log2 ratio; positive value means up-regulation in albino strain compare with parent strain.

(two genes), fungal ferroxidase (four genes) and ascomycete laccase (eight genes), respectively. Of the 14 genes, six were up-regulated in the albino mutant strain, suggesting that most of these copies could be functionally active. Indeed, the enzyme test showed significant transcription of laccase in the albino mutant compare with the parent strain (Fig. 9A) ($p < 0.05$).

In addition to DHN melanin, many fungi produce pheomelanin through the DOPA melanin pathway (Liu *et al.* 2014, Pal *et al.* 2014), in which tyrosinases or laccases generate dopaquinone either through hydroxylation of L-tyrosine, or through oxidation of DOPA. Dopaquinone auto-oxidises and polymerises to form melanins (Fig. 7A). *Fonsecaea monophora* contains 8 laccases and 2 tyrosinases coding genes (Table 3). All laccases were up-regulated in the albino mutant except for two unigenes ($p < 0.05$), as well as tyrosinases compared to the parent strain ($p > 0.05$), which matches with the following enzyme activity tests (Fig. 9A, B) and real time RT-PCR results (Fig. 9C). However, when DOPA and L-tyrosine as separated substrate were added to the medium, DOPA melanin were detected in the PDA medium with DOPA, but not L-tyrosine in both strains (Fig. 9D). These data suggested that DOPA melanin biosynthesis pathway were affected by substrate in culture medium, as well as the genes in DOPA melanin biosynthesis pathway. Indeed, in *C. neoformans*, the melanin production was regulated by specific transcript factors only in the presence of specific substrates, mainly diphenolic compounds (Chaskes & Tyndall 1978).

The pathway to produce a third type of melanin, pyomelanin (allomelanin), viz. the L-tyrosine degradation pathway (Keller *et al.* 2011), is also conserved in *F. monophora*. The two enzymes involved in this pathway are 4-hydroxyphenylpyruvate dioxygenase (*hppD*) and homogentisate dioxygenase (*hmgA*). *HppD* converts 4-hydroxyphenylpyruvate to homogentisate, which can be converted to pyomelanin through oxidation and polymerisation. Homogentisate can alternatively be degraded to other compounds by *hmgA* and two downstream enzymes, maleylacetoacetate isomerase (*maiA*) and fumarylacetoacetate hydrolase (*fahA*) (Fig. 8A). All these enzymes were found in both strains (Table 3). Interestingly, we found that *hppD* was up-regulated (3.528 fold, log2 ratio = 1.819, $p < 0.05$), while *hmgA* was down-regulated (2.156 fold, log2 ratio = −1.108, $p < 0.05$) in the albino mutant, and no significant variation in transcription levels were detected in downstream *maiA* and *fahA*, suggesting that the down-regulation of *hmgA* blocks the degradation of homogentisate, resulting in accumulation of pyomelanin. Although the real time RT-PCR results confirmed these results (Fig. 8B), the following enzyme activity test using L-tyrosine as substrate showed that pyomelanin was not detected in both strains (Fig. 9D). The possible explanation is that down-regulation of tyrosine aminotransferase (*tat*) (3.575 fold, log2 ratio = −1.910, $p < 0.05$; 3.573 fold, log2 ratio = −1.837, $p < 0.05$) attributed to the inhibition of 4-hydroxyphenylpyruvate production, result in blocking of pyomelanin biosynthesis pathway.

Please cite this article in press as: Li XQ, et al., The role of melanin pathways in extremotolerance and virulence of *Fonsecaea* revealed by *de novo* assembly transcriptomics using illumina paired-end sequencing, Studies in Mycology (2016), http://dx.doi.org/10.1016/j.simyco.2016.02.001

Table 3. Melanin biosynthesis pathway genes.

Gene	*F. monophora*			Homologues in other fungal genomes			
	Assemble gene code	Transcript level (log2 ratio) (CBS125194/ CBS122845)	*p*-Value (*<0.05)	*W. dermatitidis*	*C. carrioni*	*A. fumigatus*	*A. niger*
DHN–melanin pathway							
Polyketide synthase (Pks1)	unigene4246	−0.948	0.037*	HMPREF1120-03173	G647-03926	Afu2g17600 (Pks1)	An03g05440
	unigene4245	−0.266	0.025*		G647-03240	Afu4g00210 (EncA)	An04g09530
	unigene10003	−0.392	0.032*		G647-03914	Afu4g14560	An09g05730 (FwnA)
						Afu7g00160	An11g07310
Abhydrolase (Ayg1)	unigene1384	0.250	0.309	HMPREF1120-00377	G647-01705	Afu2g17550(Ayg1)	An14g05350 (Ayg1)
	unigene1176	0.301	0.244	HMPREF1120-02312	G647-03620		
1,3,6,8-Tetrahydroxynaphthalene reductase (Arp2)	unigene2337	−0.126	0.142	HMPREF1120-05939	G647-10180	Afu2g17560 (Arp2)	An02g00220
	unigene3830	−0.426	0.037*				
Scytalone dehydratase (Arp1)	unigene3787	−0.793	0.04*	HMPREF1120-07724	G647-03339	Afu2g17580 (Arp1)	An08g09920
Fungal pigment MCO (Abr2)	cl2088.contig1	−1.393	0.012*	HMPREF1120-02828	G647-00781	Afu2g17530 (Abr2)	An01g13660 (McoB)
	cl2088.contig2	−0.925	0.037*	HMPREF1120-05645	G647-08702	Afu1g15670	An01g14010 (McoA)
							An03g03750 (McoC)
							An04g10400 (McoO)
							An05g02540 (McoP)
Fungal ferroxidase (Abr1)	cl1408.contig1	−0.028	0.957	HMPREF1120-04510	G647-09047	Afu2g17540 (Abr1)	An14g05370 (BrnA) An01g11120 (McoE)
	cl1408.contig2	−1.865	0.013*	HMPREF1120-00173	G647-01847	Afu5g03790 (FetC)	An01g08960 (McoH)
	unigene9376	−1.874	0.027*	HMPREF1120-01590	G647-06601		An15g05520 (McoK)
	unigene9070	−1.710	0.004*	HMPREF1120-03706	G647-00377		
				HMPREF1120-04536			
DOPA–melanin pathway							
Tyrosinase (melC2)	unigene1125	0.472	0.444	HMPREF1120-05316	G647-08944	Afu3g01070	An01g09220 (MelC2)
	unigene6269	0.641	0.058	HMPREF1120-03345	G647-02663		An03g00280
				HMPREF1120-04514	G647-03851		An09g02980
					G647-09055		
Laccase (Lac)	cl2942.contig1	1.690	0.008*	HMPREF1120-05865	G647-00377	Afu4g14490	An12g05810 (McoJ)
	cl2942.contig2	1.027	0.014*	HMPREF1120-00199	G647-03384		An16g02020 (McoM)
	cl422.contig2	1.336	0.001*	HMPREF1120-08116	G647-03930		An11g03580 (McoD)
	cl31.contig1-23	−1.008	0.334	HMPREF1120-08564	G647-05054		An08g08450 (McoG)
	unigene8445	3.902	0.022*	HMPREF1120-04578	G647-00922		An05g02340 (McoF)
	unigene9375	1.717	0.016*	HMPREF1120-02754	G647-06601		An01g00860 (McoN)
	unigene3099	−0.073	0.779		G647-09047		An18g02690 (McoI)
	unigene1837	4.113	0.026*				
L-tyrosine degradation pathway							
Tyrosine aminotransferase (Tat)	cl1774.contig1	−1.910	0.003*	HMPREF1120-02164	G647-02757	Afu2g13630	An02g05540
	cl1774.contig2	−1.837	0.006*		G647-07845		
4-Hydroxyphenylpyruvate dioxygenase (hppD)	cl24.contig4	1.819	0.012*	HMPREF1120-05584	G647-06922	Afu2g04200	An11g02200
Homogentisate dioxygenase (hmgA)	unigene1219	−1.108	0.017*	HMPREF1120-03827	G647-06522	Afu2g04220	An11g02180
Fumarylacetoacetate hydrolase (fahA)	unigene2130	−0.313	0.043*	HMPREF1120-03825	G647-06520	Afu2g04230	An11g02170
					G647-09894		
Maleylacetoacetate isomerase (maiA)	unigene4460	−0.557	0.155	HMPREF1120-03438	G647-03643	Afu2g04240	An11g02160

Please cite this article in press as: Li XQ, et al., The role of melanin pathways in extremotolerance and virulence of *Fonsecaea* revealed by *de novo* assembly transcriptomics using illumina paired-end sequencing, Studies in Mycology (2016), http://dx.doi.org/10.1016/j.simyco.2016.02.001

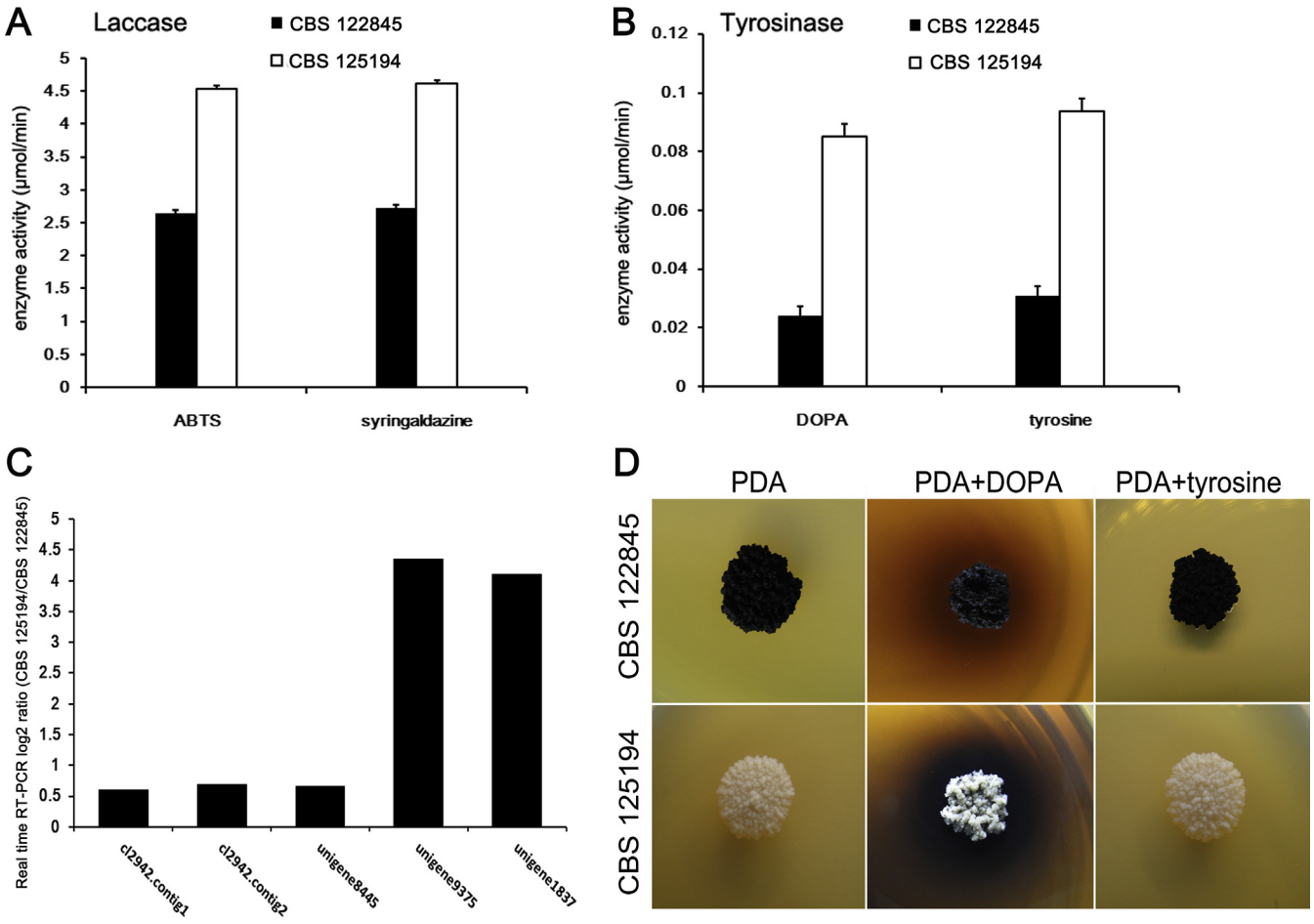

Fig. 9. The key enzyme activity test (A, B), 2,2-azino-bis-(3-ethylbenzthiazolinsulfonate) (ABTS) and syringaldazine were used as substrate of laccase activity test; DOPA and tyrosine were used as substrate of tyrosinase. Y-axis indicated the enzyme activity (micro mol/minute). Transcription levels of partial genes between two strains detected by Real time RT-PCR (C). The X-axis is the selected unigenes, Y-axis is the value of log2 ratio; positive value means up-regulation in albino strain compare with parent strain. DOPA melanin production of both strains cultured on PDA medium contained DOPA (25 mg/L) and L-tyrosine (25 mg/L), respectively (D).

To explore potential mechanism of significant down-regulation of most genes in the DHN pathway, the unique transcribed genes of each strain were collected, and the genes associated with melanin synthesis were evaluated according to archived literature. A total of 17 and 25 unigenes were uniquely transcribed in parent and albino strains, respectively (Table S2). After removing the unigenes which contained homologues in both strains, no novel genes directly linked to melanin production was uniquely transcribed in parent or albino strain. DHN-melanin deficiency in the albino strain may not be due to a sudden gain/loss of particular genes in melanin biosynthesis pathways. Melanin biosynthesis, including DHN-melanin, perhaps is regulated by multiple transcription factors. For example, melanin production of *C. neoformans* is regulated by a number of genes including cAMP signal pathway, iron regulated gene *SIT1* and chitin synthase (*Chs3*) (Zhu *et al.* 2001, Waterman *et al.* 2007). They found the key enzyme of DOPA melanin production, laccase, is synthesised in the cytoplasm, transported in vesicles, and tightly linked to the cell wall through disulfide or thioester bonds. If the strains have cell wall defects, the laccase will miss localisation of chitin-like structures, and consequently result in melanin deficiency (Walton *et al.* 2005). Our previously study in *F. monophora* already identified the cell wall defects of the albino strain by transmission electron microscopy (Zhang *et al.* 2013). Along with the up-regulation of several chitin degradation coding genes in the albino strain (Table S3), all these suggested the absence of laccase localisation is the possible mechanism of DOPA melanin deficiency in albino strains, although this needs further verification. Recently, Sapmak *et al.* (2015) found that *pbrB* gene encodes a laccase required for DHN-melanin synthesis in conidia of *Talaromyces marneffei*. Cary *et al.* (2014) found that *veA*, a sclerotium-specific pigment melanin synthesis gene, regulates asparasone in *Aspergillus flavus*. We also verified *veA* regulates asparasone synthesis in *F. monophora*, while it seems to have no effect on DHN melanin synthesis (Fig. 10). Pal *et al.* (2014) concluded that the amount and type of melanin in aspergilli largely differ from species to species. Therefore, which transcription factors are involved in regulation of DHN melanin production in *F. monophora* still needs further investigation.

Cell wall synthesis and morphogenesis

Numerous key enzymes involved in cell wall biosynthesis were identified in the transcriptome of *F. monophora* (Table S3). Chitin synthase genes encompass several subfamilies. We identified six out of seven chitin synthase genes previously described in fungi. Proteins involved in the regulation of chitin synthase activity, export of chitin synthases, and chitin degradation (chitinases) were all present in both strains. The glycosyl transferase family was also identified, while the copy number was significantly lower than in other fungi, such as *E. dermatitidis* or

Please cite this article in press as: Li XQ, et al., The role of melanin pathways in extremotolerance and virulence of *Fonsecaea* revealed by *de novo* assembly transcriptomics using illumina paired-end sequencing, Studies in Mycology (2016), http://dx.doi.org/10.1016/j.simyco.2016.02.001

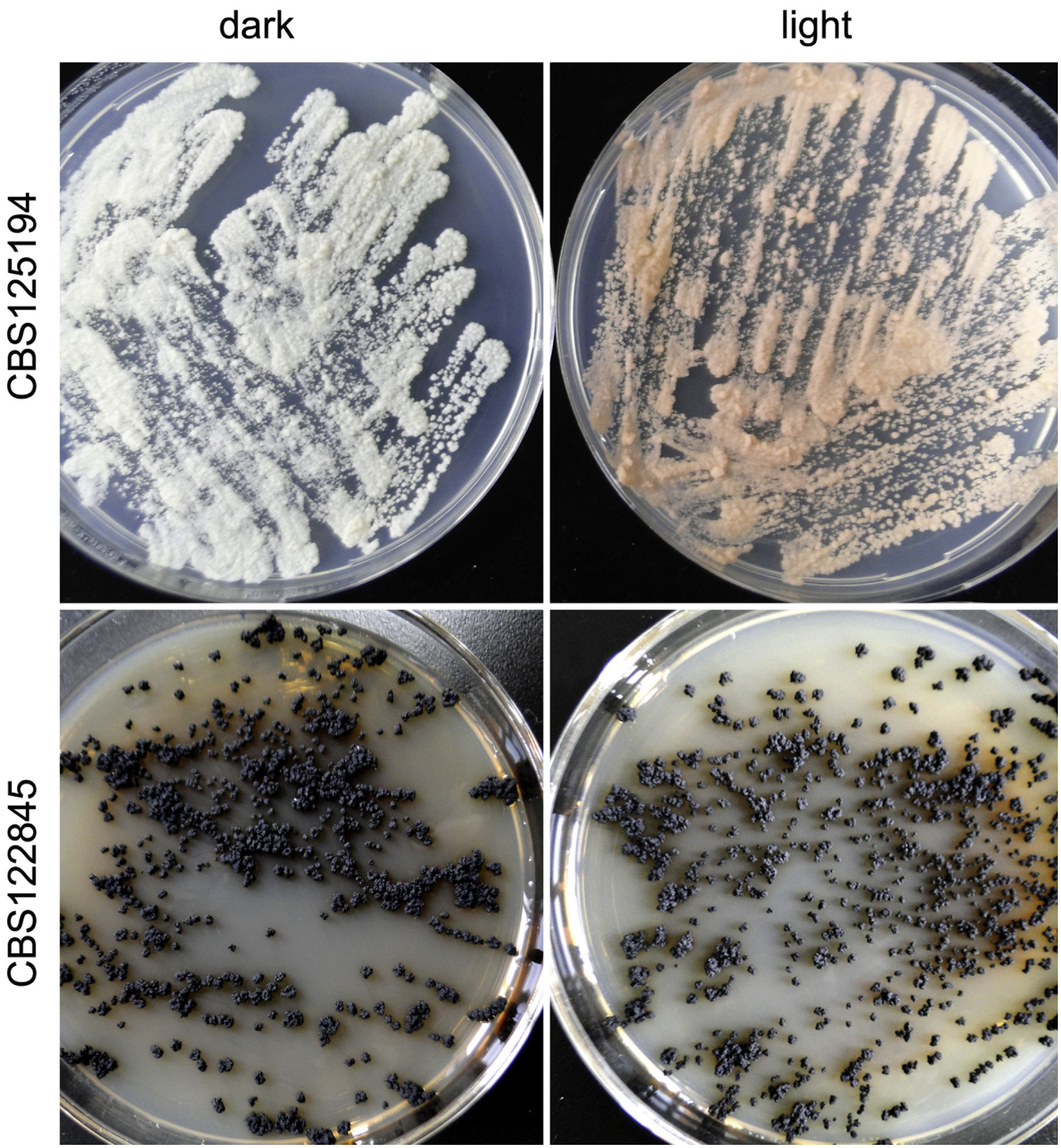

Fig. 10. Effects of light on pigment and carotenoid biosynthesis. Both strains were grown on PDA agar medium exposing to light or keep in dark, and both cultures were incubated at 25 °C for 7 days.

Aspergillus (Chen *et al.* 2014). Glucanases (β-1,3-glucanase, β-1,4-glucanase, endo and exo-glucanases) and GlcNAc-mannosyltransferase genes, which are important enzymes in glucan synthesis, were also observed in both transcriptomes (Table S3). Although transcript levels of partial chitin synthase coding genes were up-regulated in albino strain, some chitin degradation coding genes, e.g. chitinase, were also up-regulated, as well as numbers of β-1,3-glucan synthesis and regulation genes including β-1,3-transglucosylases and trans-glycosidases (Table S3, Fig. S2), which probably suggested a change of cell wall components and increasing cross linking beta-glucan to chitin in albino strain.

Alpha-1,3-glucanases play a key role in biosynthesis of α-1,3-glucan which normally transcript in yeast form of pathogenic fungi, such as *Histoplasma capsulatum* and *Aspergillus* species. The archived studies showed that α-1,3-glucan helps to mask β-glucans from detection by the host receptor dectin-1, and results in immunological escape (Aimanianda *et al.* 2009, Fujikawa *et al.* 2012). In contrast, α-1,3-glucanase is able to remove this α-glucan mask by catalysing the degradation of α-1,3-glucan. Both α-1,3-glucan synthases (*Ags* family) and α-1,3-glucanases (*Agn* family) was identified in *F. monophora,* as well as *F. pedrosoi* and *F. multimorphosa* genomes, while not detected in *E. dermatitidis* (Chen *et al.* 2014). Interestingly, both *Ags* and

Please cite this article in press as: Li XQ, et al., The role of melanin pathways in extremotolerance and virulence of *Fonsecaea* revealed by *de novo* assembly transcriptomics using illumina paired-end sequencing, Studies in Mycology (2016), http://dx.doi.org/10.1016/j.simyco.2016.02.001

Agn families are present as multiple copies in *Histoplasma capsulatum*, *Magnaporthe oryzae*, and *Aspergillus* species (Rappleye *et al.* 2007, Aimanianda *et al.* 2009, Fujikawa *et al.* 2012). This variation in α-1,3-glucan biosynthesis of *F. monophora* might affect the interactions potentially between this pathogen and the host's immune system. That is because the knock-out of *Ags* significantly up regulated the recognition of host cell, and results in the attenuate of pathogenesis of *A. fumigatus* and *M. oryzae*. Therefore, we speculated the deficiency of melanin, up-regulated chitin degradation coding genes and β-1,3-glucan synthesis genes in albino strain perhaps promote the recognised by host immune cell (Fig. 11), and results in sufficient killing factor secretion of host cells, consequently, leading to clear of infection. In contrast, insufficient exposing of antigens (β-1,3-glucan) due to shield effects of α-1,3-glucan and melanin probably caused a chronic infection in parent strain (Fig. 11). Our previously studies in a marine macrophage infection model (Zhang *et al.* 2013), as well as animal infection model (unpublished data) confirmed this speculation.

Another class of enzymes, α-amylases, performing transglycosylation or hydrolysis of glycosidic linkages, is present in *F. monophora*. Moreover, both intracellular and secreted α amylases were identified simultaneously, as well as in many other fungi (van der Kaaij *et al.* 2007). In addition, similar to

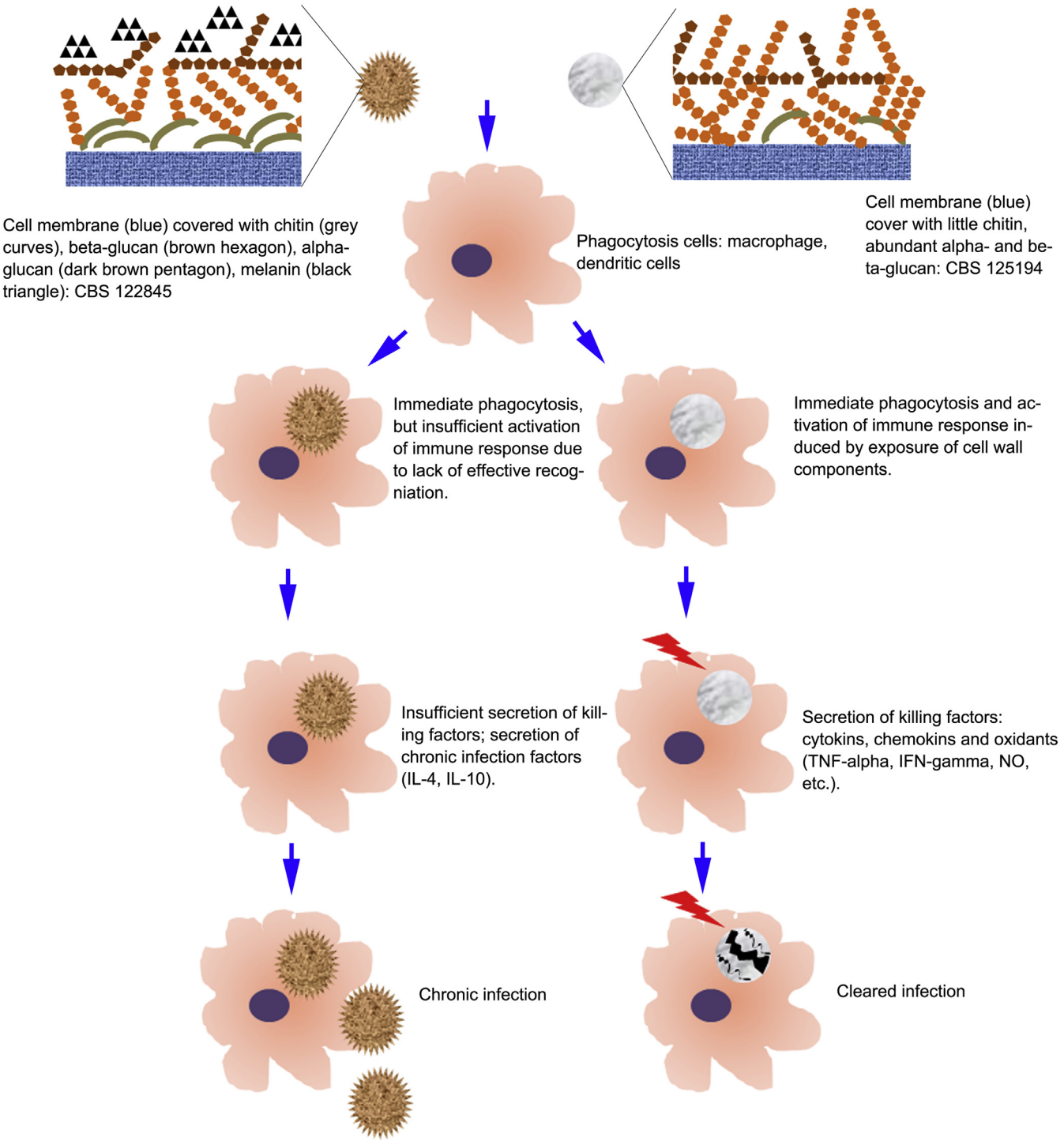

Fig. 11. The speculated working cartoon model explaining differential immune events between parent and albino strains. The exposure of the glycoprotein layer (β-1,3-glucan) on the albino cell wall promote the host immunological response, while the melanin, α-1,3-glucan probably hides the β-1,3-glucan antigens, and results in chronic immune response of host cell.

Please cite this article in press as: Li XQ, et al., The role of melanin pathways in extremotolerance and virulence of *Fonsecaea* revealed by *de novo* assembly transcriptomics using illumina paired-end sequencing, Studies in Mycology (2016), http://dx.doi.org/10.1016/j.simyco.2016.02.001

E. dermatitidis and *Schizosaccharomyces pombe*, *F. monophora* lacks copies of conserved chitosinases, whereas they exist ordinarily in genome of other filamentous fungi, including *A. fumigatus*, *A. niger*, *A. flavus*, *Coccidioides immitis*, *Trichophyton rubum* and *Neurospora crassa* (Shimono *et al.* 2002, Martinez *et al.* 2012, Chen *et al.* 2014).

The genetic mechanisms of activating developmental dimorphic switches in other pathogenic fungi have been clarified, e.g. *Candida albicans* (Biswas *et al.* 2007). Several gene homologues coding for morphology regulatory enzymes were identified in both transcriptomes of *F. monophora*, including mitogen-activated protein kinase family, cell division cycle protein family (*CDC5*, *CDC42*) and Ras family [a protein superfamily of small GTPases which function independently as hydrolase enzymes to bind to and hydrolyse a guanosine triphosphate (GTP) to form guanosine diphosphate (GDP)] (Table S4). Some key genes encoding important transcription factors which regulate the developmental switches from yeast to hyphae were present in the transcriptome of *F. monophora*, including APSES transcription factors (Wang & Szaniszlo 2007, Qi *et al.* 2012, Connolly *et al.* 2013) and STE transcription factor (Biswas *et al.* 2007). Since dimorphic switches between the muriform cell and hyphae were never detected in any of the strains, it seems that this process was regulated by an unidentified transcription factor; thus further genome wide extension study are needed.

Light-sensing and pigment production

Fungi have multiple sensors that respond to light of different wavelengths. Genes associated with light sensing were also identified in both *F. monophora* strains, including the velvet family of regulatory genes (*veA*, *velB*, *velC* and *vosA*) which play a key role in coordinating development and secondary metabolism responding to light. Opsin-like protein is one of the members of light sensors which is conserved in carotenoid biosynthetic pathway and cryptochrome-photolyase that responds to UV-A light. Several fungi lost the homologues of Opsin-like protein, including *T. rubrum* and *C. immitis* (Idnurm *et al.* 2010), while *F. monophora* contains this class of light sensing proteins (Table S5). Colonies of the albino strain showed increased pink colour when incubated under light, while it maintained its white colour when incubated in the dark, indicating production of carotenoids (Fig. 10). The coordination of these responses would enable protection against and response to light stimuli as observed in *Exophiala dermatitidis* (Chen *et al.* 2014).

Environmental stress

In pathogenic fungi, several genes were proven to be involved in the resistance to the environmental stress from the host cells, including superoxide dismutase (SOD), catalase, NADH dehydrogenase, members of *Hog1* family and the transcriptional regulator *Skn7p* (Abad *et al.* 2010). Most of those genes were identified in the transcriptomes of *F. monophora* (Table S6, Fig. S2). Numerous transcripts were homologues of genes encoding enzymes in resistance to oxidants, irradiation and extreme temperatures. In addition, heat shock proteins (HSPs) and heat shock factors (HSFs), which serve as chaperones to couple with target proteins and activators of HSPs, respectively, were identified in both transcriptomes. However, the transcription levels of those genes were comparable because the same medium and culture conditions were used for both strains. Only the cl1296.contig4 and unigene8441, which coding superoxide dismutase and deoxyribodipyrimidine photo-lyase resistant to oxidants and UV-A damage, respectively, were significantly down-regulated in the albino mutant (16.167 fold, log2 ratio = −4.015, $p < 0.05$; 4.95 fold, log2 ratio = −2.307, $p < 0.05$) (Tables S5 and S6). These results were concordant with our previous finding that the albino strain was sensitive to oxidants and UV light (Sun *et al.* 2011). However, since no pairwise experiments were done under different conditions of oxidants, temperature and pH were done, stress tolerance were not detected, thus no significant transcription difference was to be expected between the strains.

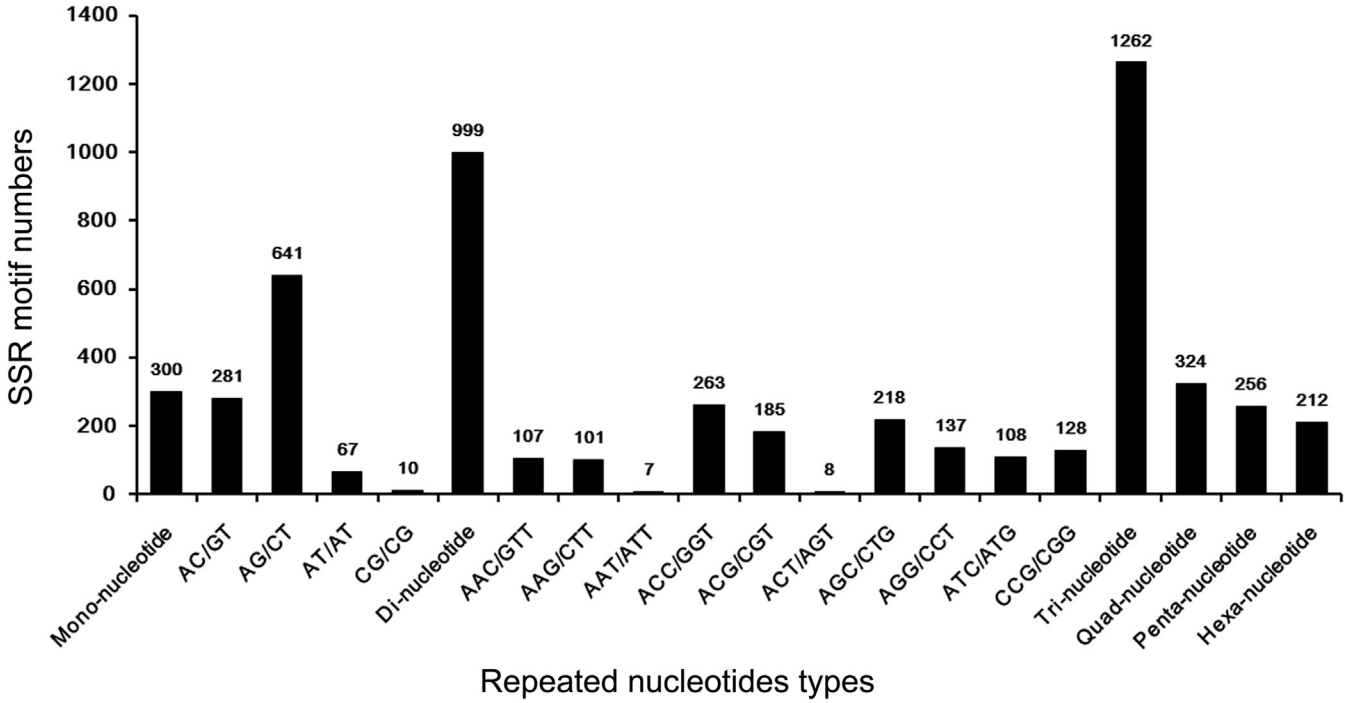

Fig. 12. Frequency distribution of cSSRs based on motif sequence types. The X-axis is the repeated nucleotides types, and Y-axis is the SSR motif numbers in total.

Please cite this article in press as: Li XQ, et al., The role of melanin pathways in extremotolerance and virulence of *Fonsecaea* revealed by *de novo* assembly transcriptomics using illumina paired-end sequencing, Studies in Mycology (2016), http://dx.doi.org/10.1016/j.simyco.2016.02.001

Frequency and distribution of EST-SSRs in the same transcriptome

In total, 2 849 sequences containing 3 353 SSRs were identified from 21 600 consensus sequences, and 425 of the sequences contained more than one SSR. The SSR frequency in the consensus transcriptome was 13.18 %. The distribution density was 67.33 per Mb. The most abundant type of repeat motif was trinucleotide (36.69 %), followed by dinucleotide (30.25 %), quadnucleotide (9.81 %), mononucleotide (9.08 %), pentanucleotide (7.75 %) and hexanucleotide repeat units (6.62 %) (Table S7). SSRs with five tandem repeats (27.39 %) were the most common, followed by six tandem repeats (23.41 %), >10 tandem repeats (13.50 %) and seven tandem repeats (12.29 %) (Table S7). The dominant repeat motif in SSRs was AG/CT, followed by AC/GT, ACC/GGT, AGC/CTG, and ACG/CGT (Fig. 12).

CONCLUSIONS

This study investigated the transcriptome profiles of melanised and albino strains of *F. monophora* using Illumina RNA-seq and DGE deep sequencing technologies. The substantial amount of transcripts obtained revealed the genes involved in melanin biosynthesis in *F. monophora*, and suggested the loss of melanin in albino mutant is most likely due to blocking of the DNH pathway. Moreover, most of the genes involved in light sensing, cell wall synthesis, morphology regulation and tolerance to environmental stress (UV, pH, temperature, oxidants, and osmotic condition) were assembled and annotated in transcriptomes of *F. monophora*. The thousands of cSSR markers produced in this study will enable genetic linkage mapping construction and gene-based association studies.

ACKNOWLEDGEMENTS

This work was supported by grants from the National Natural Science Foundation of China (81301411), the Nature Science Foundation of Guangdong Province, China (S2013010013175; S2013010013175) and the Medical Scientific Research Foundation of Guangdong Province, China (B2013082). V.A. Vicente received fellowships from National Council for Scientific and Technological Development (CNPq), Brasilia, Brazil.

APPENDIX A. SUPPLEMENTARY DATA

Supplementary data related to this article can be found at http://dx.doi.org/10.1016/j.simyco.2016.02.001.

REFERENCES

Abad A, Fernández-Molina JV, Bikandi J, *et al*. (2010). What makes *Aspergillus fumigatus* a successful pathogen? Genes and molecules involved in invasive aspergillosis. *Revista Iberoamericana de Micologia* **27**: 155–182.

Aimanianda V, Bayry J, Bozza S, *et al*. (2009). Surface hydrophobin prevents immune recognition of airborne fungal spores. *Nature* **460**: 1117–1121.

Anisimov SV (2008). Serial Analysis of Gene Expression (SAGE): 13 years of application in research. *Current Pharmacology and Biotechnology* **9**: 338–350.

Attapattu MC (1997). Chromoblastomycosis – a clinical and mycological study of 71 cases from Sri Lanka. *Mycopathologia* **137**: 145–151.

Audic S, Claverie JM (1997). The significance of digital gene expression profiles. *Genome Research* **7**: 986–995.

Benjamini Y, Drai D, Elmer G, *et al*. (2001). Controlling the false discovery rate in behavior genetics research. *Behavioural Brain Research* **125**: 279–284.

Biswas S, van Dijck P, Datta A (2007). Environmental sensing and signal transduction pathways regulating morphopathogenic determinants of *Candida albicans*. *Microbiological and Molecular Biology Reviews* **71**: 348–376.

de Bruijn NG (1946). A combinatorial problem. *Proceedings of the Koninklijke Nederlandse Akademie van Wetenschappen* **49**: 758–764.

Cary JW, Harris-Coward PY, Ehrlich KC, *et al*. (2014). Functional characterization of a *veA*-dependent polyketide synthase gene in *Aspergillus flavus* necessary for the synthesis of asparasone, a sclerotium-specific pigment. *Fungal Genetics and Biology* **64**: 25–35.

Chaskes S, Cammer M, Nieves E, *et al*. (2014). Pigment production on L-tryptophan medium by *Cryptococcus gattii* and *Cryptococcus neoformans*. *PLoS One* **9**: e91901.

Chaskes S, Tyndall RL (1978). Pigment production by *Cryptococcus neoformans* and other *Cryptococcus* species from aminophenols and diaminobenzenes. *Journal of Clinical Microbiology* **7**: 146–152.

Chen ZH, Martinez DA, Gujja S, *et al*. (2014). Comparative genomic and transcriptomic analysis of *Wangiella dermatitidis*, a major cause of phaeohyphomycosis and a model black yeast human pathogen. *G3 (Bethesda)* **4**: 561–578.

Conesa A, Gotz S, Garcia-Gomez JM, *et al*. (2005). Blast2GO: a universal tool for annotation, visualization and analysis in functional genomics research. *Bioinformatics* **21**: 3674–3676.

Connolly LA, Riccombeni A, Grozer Z, *et al*. (2013). The APSES transcription factor *Efg1* is a global regulator that controls morphogenesis and biofilm formation in *Candida parapsilosis*. *Molecular Microbiology* **90**: 36–53.

Cunha MM, Franzen AJ, Alviano DS, *et al*. (2005). Inhibition of melanin synthesis pathway by tricyclazole increases susceptibility of *Fonsecaea pedrosoi* against mouse macrophages. *Microscopy Research and Technique* **68**: 377–384.

Esterre P, Andriantsimahavandy A, Ramarcel ER, *et al*. (1996). Forty years of chromoblastomycosis in Madagascar: a review. *American Journal of Tropical Medicine and Hygiene* **55**: 45–47.

Farbiarz SR, de Carvalho TU, Alviano C, *et al*. (1992). Inhibitory effect of melanin on the interaction of *Fonsecaea pedrosoi* with mammalian cells *in vitro*. *Journal of Medical and Veterinary Mycology* **30**: 265–273.

Franzen AJ, Cunha MM, Batista EJ, *et al*. (2006). Effects of tricyclazole (5-methyl-1,2,4-triazol[3,4] benzothiazole), a specific DHN-melanin inhibitor, on the morphology of *Fonsecaea pedrosoi* conidia and sclerotic cells. *Microscopy Research and Technology* **69**: 729–737.

Fujikawa T, Sakaguchi A, Nishizawa Y, *et al*. (2012). Surface α-1,3-glucan facilitates fungal stealth infection by interfering with innate immunity in plants. *PLoS Pathogens* **8**: e1002882.

Gomez BL, Nosanchuk JD, Diez S, *et al*. (2001). Detection of melanin-like pigments in the dimorphic fungal pathogen *Paracoccidioides brasiliensis in vitro* and during infection. *Infection and Immunity* **69**: 5760–5767.

Grabherr MG, Haas BJ, Yassour M, *et al*. (2011). Full-length transcriptome assembly from RNA-Seq data without a reference genome. *Nature Biotechnology* **29**: 644–652.

de Hoog GS, Attili-Angelis D, Vicente VA, *et al*. (2004). Molecular ecology and pathogenic potential of *Fonsecaea* species. *Medical Mycology* **42**: 405–416.

Idnurm A, Verma S, Corrochano LM (2010). A glimpse into the basis of vision in the kingdom *Mycota*. *Fungal Genetics and Biology* **47**: 881–892.

Iseli C, Jongeneel CV, Bucher P (1999). ESTScan: a program for detecting, evaluating, and reconstructing potential coding regions in EST sequences. *Proceedings of the International Conference on Intelligent Systems for Molecular Biology*, 138–148.

Jacobson ES (2000). Pathogenic roles for fungal melanins. *Clinical Microbiology Reviews* **13**: 708–717.

van der Kaaij RM, Janecek S, van der Maarel MJ, *et al*. (2007). Phylogenetic and biochemical characterization of a novel cluster of intracellular fungal α-amylase enzymes. *Microbiology* **153**: 4003–4015.

Kanehisa M, Araki M, Goto S, *et al*. (2008). KEGG for linking genomes to life and the environment. *Nucleic Acids Research* **36**: D480–D484.

Keller S, Macheleidt J, Scherlach K, *et al*. (2011). Pyomelanin formation in *Aspergillus fumigatus* requires *HmgX* and the transcriptional activator *HmgR* but is dispensable for virulence. *PLoS One* **6**: e26604.

Kogej T, Wheeler MH, Lanisnik Rizner T, *et al*. (2004). Evidence for 1,8-dihydroxynaphthalene melanin in three halophilic black yeasts grown under saline and non-saline conditions. *FEMS Microbiology Letters* **232**: 203–209.

Please cite this article in press as: Li XQ, et al., The role of melanin pathways in extremotolerance and virulence of *Fonsecaea* revealed by *de novo* assembly transcriptomics using illumina paired-end sequencing, Studies in Mycology (2016), http://dx.doi.org/10.1016/j.simyco.2016.02.001

Kombila M, Gomez de Diaz M, Richard-Lenoble D, *et al*. (1995). Chromoblastomycosis in Gabon. Study of 64 cases. *Santé* **5**: 235–244.
Langfelder K, Streibel M, Jahn B, *et al*. (2003). Biosynthesis of fungal melanins and their importance for human pathogenic fungi. *Fungal Genetics and Biology* **38**: 143–158.
Laufer Z, Beckett RP, Minibayeva FV (2006). Co-occurrence of the multicopper oxidases tyrosinase and laccase in lichens in sub-order peltigerineae. *Annals of Botany* **98**: 1035–1042.
Liang C, Liu X, Yiu SM, *et al*. (2013). *De novo* assembly and characterization of *Camelina sativa* transcriptome by paired-end sequencing. *BMC Genomics* **14**: 146.
Liu GQ, Li WS, Zheng PH, *et al*. (2012). Transcriptomic analysis of 'Suli' pear (*Pyrus pyrifolia* white pear group) buds during the dormancy by RNA-Seq. *BMC Genomics* **13**: 700.
Liu DH, Wei L, Guo T, *et al*. (2014). Detection of DOPA-melanin in the dimorphic fungal pathogen *Penicillium marneffei* and its effect on macrophage phagocytosis *in vitro*. *PLoS One* **9**: e92610.
Liu HF, Xi LY, Zhang JM, *et al*. (2007). Identifying differentially expressed genes in the dimorphic fungus *Penicillium marneffei* by suppression subtractive hybridization. *FEMS Microbiology Letters* **270**: 97–103.
Martinez DA, Oliver BG, Gräser Y, *et al*. (2012). Comparative genome analysis of *Trichophyton rubrum* and related dermatophytes reveals candidate genes involved in infection. *MBio* **3** e00259-00212.
Morozova O, Marra MA (2008). Applications of next-generation sequencing technologies in functional genomics. *Genomics* **92**: 255–264.
Morris-Jones R, Gomez BL, Diez S, *et al*. (2005). Synthesis of melanin pigment by *Candida albicans in vitro* and during infection. *Infection and Immunity* **73**: 6147–6150.
Mortazavi A, Williams BA, McCue K, *et al*. (2008). Mapping and quantifying mammalian transcriptomes by RNA-Seq. *Nature Methods* **5**: 621–628.
Nagalakshmi U, Wang Z, Waern K, *et al*. (2008). The transcriptional landscape of the yeast genome defined by RNA sequencing. *Science* **320**: 1344–1349.
Najafzadeh MJ, Sun JF, Vicente VA, *et al*. (2011). Molecular epidemiology of *Fonsecaea* species. *Emerging Infectious Diseases* **17**: 464–469.
Nosanchuk JD, Casadevall A (2003). The contribution of melanin to microbial pathogenesis. *Cell Microbiology* **5**: 203–223.
Nosanchuk JD, van Duin D, Mandal P, *et al*. (2004). *Blastomyces dermatitidis* produces melanin *in vitro* and during infection. *FEMS Microbiology Letters* **239**: 187–193.
Nosanchuk JD, Gomez BL, Youngchim S, *et al*. (2002). *Histoplasma capsulatum* synthesizes melanin-like pigments *in vitro* and during mammalian infection. *Infection and Immunity* **70**: 5124–5131.
Nosanchuk JD, Rosas AL, Casadevall A (1998). The antibody response to fungal melanin in mice. *Journal of Immunology* **160**: 6026–6031.
Pal AK, Gajjar DU, Vasavada AR (2014). DOPA and DHN pathway orchestrate melanin synthesis in *Aspergillus* species. *Medical Mycology* **52**: 10–18.
Pindycka-Piaszczynska M, Krzysciak P, Piaszczynski M, *et al*. (2014). Chromoblastomycosis as an endemic disease in temperate Europe: first confirmed case and review of the literature. *European Journal Clinical Microbiology Infectious Diseases* **33**: 391–398.
Polak A, Dixon DM (1989). Loss of melanin in *Wangiella dermatitidis* does not result in greater susceptibility to antifungal agents. *Antimicrobial Agents and Chemotherapy* **33**: 1639–1640.
Qi ZQ, Wang Q, Dou XY, *et al*. (2012). MoSwi6, an APSES family transcription factor, interacts with *MoMps1* and is required for hyphal and conidial morphogenesis, appressorial function and pathogenicity of *Magnaporthe oryzae*. *Molecular Plant Pathology* **13**: 677–689.
Queiroz-Telles F, Esterre P, Perez-Blanco M, *et al*. (2009). Chromoblastomycosis: an overview of clinical manifestations, diagnosis and treatment. *Medical Mycology* **47**: 3–15.
Rappleye CA, Eissenberg LG, Goldman WE (2007). *Histoplasma capsulatum* α-(1,3)-glucan blocks innate immune recognition by the β-glucan receptor. *Proceedings of the National Academy of Sciences of the USA* **104**: 1366–1370.
Romero-Martinez R, Wheeler M, Guerrero-Plata A, *et al*. (2000). Biosynthesis and functions of melanin in *Sporothrix schenckii*. *Infection and Immunity* **68**: 3696–3703.
Ruiz-Diez B, Martinez-Suarez JV (2003). Isolation, characterization, and antifungal susceptibility of melanin-deficient mutants of *Scedosporium prolificans*. *Current Microbiology* **46**: 228–232.
van de Sande WW, de Kat J, Coppens J, *et al*. (2007). Melanin biosynthesis in *Madurella mycetomatis* and its effect on susceptibility to itraconazole and ketoconazole. *Microbes and Infection* **9**: 1114–1123.
Santos AL, Palmeira VF, Rozental S, *et al*. (2007). Biology and pathogenesis of *Fonsecaea pedrosoi*, the major etiologic agent of chromoblastomycosis. *FEMS Microbiology Reviews* **31**: 570–591.
Sapmak A, Boyce KJ, Andrianopoulos A, *et al*. (2015). The *pbrB* gene encodes a laccase required for DHN-melanin synthesis in conidia of *Talaromyces (Penicillium) marneffei*. *PLoS One* **10**: e0122728.
Schnitzler N, Peltroche-Llacsahuanga H, Bestier N, *et al*. (1999). Effect of melanin and carotenoids of *Exophiala (Wangiella) dermatitidis* on phagocytosis, oxidative burst, and killing by human neutrophils. *Infection and Immunity* **67**: 94–101.
Shimono K, Matsuda H, Kawamukai M (2002). Functional expression of chitinase and chitosanase, and their effects on morphologies in the yeast *Schizosaccharomyces pombe*. *Bioscience, Biotechnology and Biochemistry* **66**: 1143–1147.
Silva JP, de Souza W, Rozental S (1998). Chromoblastomycosis: a retrospective study of 325 cases on Amazonic Region (Brazil). *Mycopathologia* **143**: 171–175.
Sultan M, Schulz MH, Richard H, *et al*. (2008). A global view of gene activity and alternative splicing by deep sequencing of the human transcriptome. *Science* **321**: 956–960.
Sun JF, Li XQ, Feng PY, *et al*. (2014). RNAi-mediated silencing of fungal acuD gene attenuates the virulence of *Penicillium marneffei*. *Medical Mycology* **52**: 167–178.
Sun JF, Najafzadeh MJ, Gerrits van den Ende AHG, *et al*. (2012). Molecular characterization of pathogenic members of the genus *Fonsecaea* using multilocus analysis. *PLoS One* **7**: e41512.
Sun JF, Zhang JM, Najafzadeh MJ, *et al*. (2011). Melanization of a meristematic mutant of *Fonsecaea monophora* increases tolerance to stress factors while no effects on antifungal susceptibility. *Mycopathologia* **172**: 373–380.
Surash S, Tyagi A, de Hoog GS, *et al*. (2005). Cerebral phaeohyphomycosis caused by *Fonsecaea monophora*. *Medical Mycology* **43**: 465–472.
Thornton CR, Ryder LS, Le Cocq K, *et al*. (2015). Identifying the emerging human pathogen *Scedosporium prolificans* by using a species-specific monoclonal antibody that binds to the melanin biosynthetic enzyme tetrahydroxynaphthalene reductase. *Environmental Microbiology* **17**: 1023–1038.
Tsai HF, Fujii I, Watanabe A, *et al*. (2001). Pentaketide melanin biosynthesis in *Aspergillus fumigatus* requires chain-length shortening of a heptaketide precursor. *Journal of Biological Chemistry* **276**: 29292–29298.
Wang Q, Szaniszlo PJ (2007). *WdStuAp*, an APSES transcription factor, is a regulator of yeast-hyphal transitions in *Wangiella (Exophiala) dermatitidis*. *Eukaryotic Cell* **6**: 1595–1605.
Wang Z, Gerstein M, Snyder M (2009). RNA-Seq: a revolutionary tool for transcriptomics. *Nature Reviews Genetics* **10**: 57–63.
Walton FJ, Idnurm A, Heitman J (2005). Novel gene functions required for melanization of the human pathogen *Cryptococcus neoformans*. *Molecular Microbiology* **57**: 1381–1396.
Waterman SR, Hacham M, Panepinto J, *et al*. (2007). Cell wall targeting of laccase of *Cryptococcus neoformans* during infection of mice. *Infection and Immunity* **75**: 714–722.
Wei WL, Qi XQ, Wang LH, *et al*. (2011). Characterization of the sesame (*Sesamum indicum* L.) global transcriptome using Illumina paired-end sequencing and development of EST-SSR markers. *BMC Genomics* **12**: 451.
Wheeler MH, Abramczyk D, Puckhaber LS, *et al*. (2008). New biosynthetic step in the melanin pathway of *Wangiella (Exophiala) dermatitidis*: evidence for 2-acetyl-1,3,6,8-tetrahydroxynaphthalene as a novel precursor. *Eukaryotic Cell* **7**: 1699–1711.
Xi LY, Lu CM, Sun JF, *et al*. (2009a). Chromoblastomycosis caused by a meristematic mutant of *Fonsecaea monophora*. *Medical Mycology* **47**: 77–80.
Xi LY, Sun JF, Lu CM, *et al*. (2009b). Molecular diversity of *Fonsecaea (Chaetothyriales)* causing chromoblastomycosis in southern China. *Medical Mycology* **47**: 27–33.
Xiang LX, He D, Dong WR, *et al*. (2010). Deep sequencing-based transcriptome profiling analysis of bacteria-challenged *Lateolabrax japonicus* reveals insight into the immune-relevant genes in marine fish. *BMC Genomics* **11**: 472.
Ye J, Fang L, Zheng HK, *et al*. (2006). WEGO: a web tool for plotting GO annotations. *Nucleic Acids Research* **34**: W293–W297.
Zhang JM, Wang L, Xi LY, *et al*. (2013). Melanin in a meristematic mutant of *Fonsecaea monophora* inhibits the production of nitric oxide and Th1 cytokines of murine macrophages. *Mycopathologia* **175**: 515–522.
Zhu XD, Gibbons J, Garcia-Rivera J, *et al*. (2001). Laccase of *Cryptococcus neoformans* is a cell wall-associated virulence factor. *Infection and Immunity* **69**: 5589–5596.

Please cite this article in press as: Li XQ, et al., The role of melanin pathways in extremotolerance and virulence of *Fonsecaea* revealed by *de novo* assembly transcriptomics using illumina paired-end sequencing, Studies in Mycology (2016), http://dx.doi.org/10.1016/j.simyco.2016.02.001